Chapter-4

Blank page

4. Tribological performance of various grades of PAOs with COOH-functionalized MWCNTs as an additive

This chapter emphasizes the tribological performances of COOH-functionalized MWCNTs dispersed in different grades of polyalphaolefins (i.e., PAO 4, PAO 6, PAO 40, and PAO 100) and polypropylene glycol (i.e., PPG 2000). The friction and wear properties have been estimated using a four-ball tribometer and SRV5 tribometer under fully flooded and starved lubrication conditions, respectively. The COOH-functionalized MWCNTs were characterized by X-ray diffractometer (XRD), high-resolution transmission electron microscopy (HR-TEM), and Fourier-transform infrared spectroscopy (FTIR). The tribological test results showed that with the addition of MWCNTs, the friction and wear properties of nanolubricants had improved significantly compared to the plain oils. For the better unveiling of the lubrication mechanism of MWCNTs, worn surfaces were characterized using various analytical techniques such as scanning electron microscopy (SEM), scanning probe microscope (SPM), energy-dispersive X-ray spectroscopy (EDS), and X-ray photoelectron microscopy (XPS).

4.1. Part-A: Tribological investigation of PAOs-based nanolubricants under fully flooded lubrication conditions using four-ball tribo-testing

4.1.1. Structural and Morphological Attributes of COOH-Functionalized MWCNTs

The XRD spectrum of MWCNTs, as displayed in **Figure 4.1(a)**, showed the intense and acute reflection peak (002) at an angle of 26.5º with an interlayer spacing of 0.34 nm. The other typical peaks were found at an angle of 42.6º, 53.5º, and 77.5º, which appertains to (100), (004), and (110) planes, respectively. The acquired XRD spectra of MWCNTs corroborated the excellent compliance with JCPDS reference code 00-008-0415 and affirmed the crystalline and hexagonal graphitic structure of MWCNTs. The peak 002 emerges in the XRD profile due to the interlayer heaping of a graphene sheet. It implies that graphene sheets are embedded together in the form of a coaxial cylinder and demonstrate the features of multiwall [126,127].

Fig. 4.1(b) depicts the FTIR spectra of COOH-functionalized MWCNTs. A broad peak at 3432 cm^{-1} has been attributed to the vibration of the O-H group [128]. The carbonyl group (C=O) was detected at 1717 cm^{-1} [129]. The peak obtained at 1580 cm^{-1} is associated with the stretching modes of the aromatic C=C bond, which arose due to oxygenated function groups. After that, the bond symmetry disappears [62]. Furthermore, the peaks spotted at 1167 cm^{-1} and 2927 cm^{-1} are attributed to C-O (stretching mode of phenol and carboxyl group) and the symmetric stretching vibration of C-H [130,131]. The above results of FTIR validate that the COOH groups are successfully affixed on the exterior of MWCNTs.

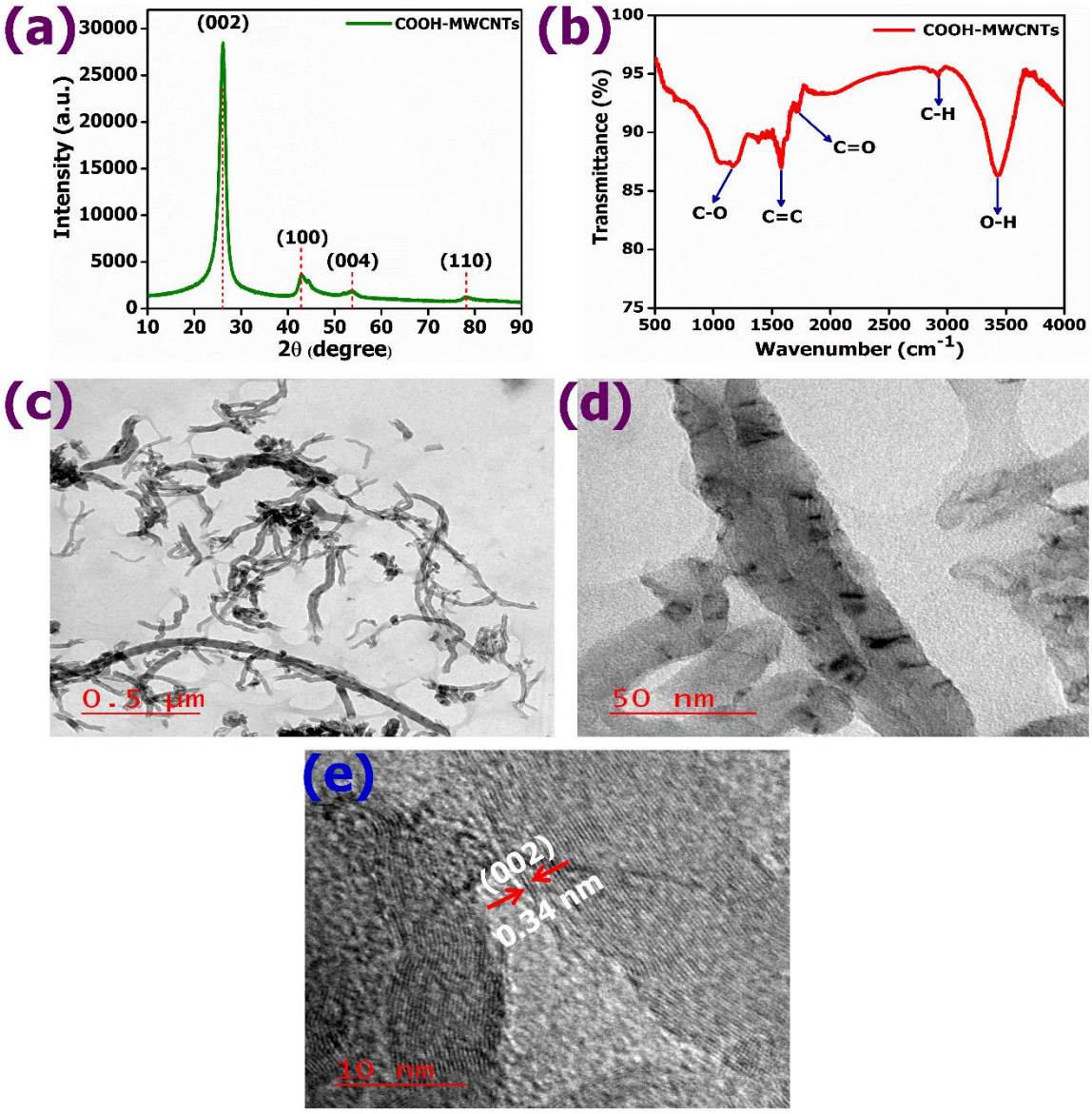

Figure 4.1: (a) XRD pattern, (b) FTIR spectra, and (c–e) HR-TEM micrographs of COOH-functionalized MWCNTs

The nanostructure of MWCNTs was analysed by HR-TEM, and low and high-resolution micrographs of HR-TEM are shown in **Figures 4.1(c)- 4.1(e)**. The low-resolution image (**Figure 4.1(c)**) revealed rod-type morphological characteristics. Whereas hollow tubular characteristics of MWCNTs with proximately 30–35 annular layers are manifested in higher resolution TEM images (**Figures 4.1(d)** and **4.1(e)**). With the help of IMAGE J software, the diameter of MWCNTs was measured. The variation in the outer diameter of MWCNTs with the number of counts is given in **Figure 4.2(a)**. The average outer diameter of the additive was observed to be ~20 nm, and the diameter distribution was in the range

of 9 to 35 nm. **Figure 4.2(b)** displays the size vs frequency distribution of MWCNTs, and most of the MWCNTs were in the range between 10-30 nm.

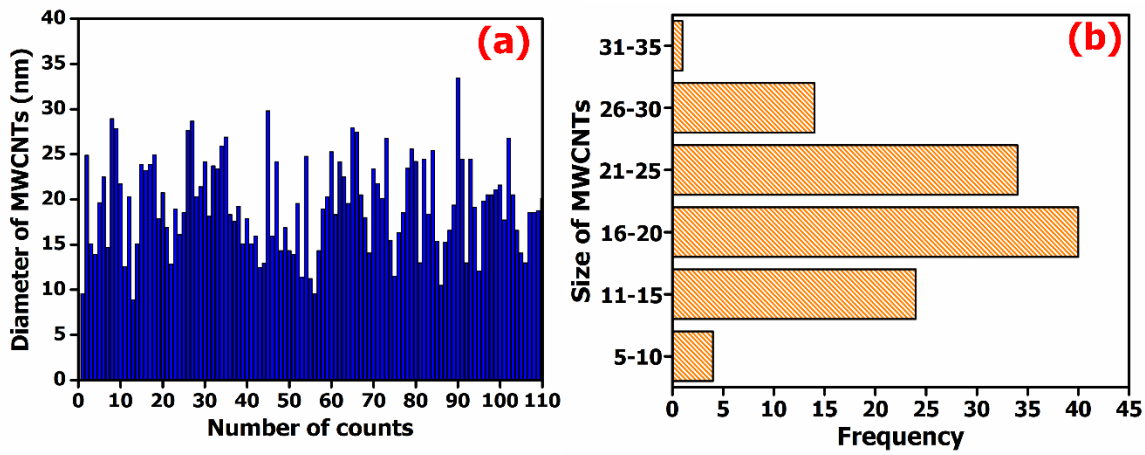

Figure 4.2: (a) Variation in the diameter of MWCNTs, and (b) size and frequency distribution of additive

4.1.2. Tribological Performance of nanolubricants

4.1.2.1. Antifriction behaviour of nanolubricants

The friction behaviour of different grades of PAOs with varying compositions of MWCNTs has been shown in **Figure 4.3**. The variation in COF with time at an optimum concentration of MWCNTs as an additive in PAO 4, PAO 6, PAO 40, and PAO 100 is presented in **Figure 4.3(a)**. It is shown in Figure 4.3(a) that a maximum variation in COF has been observed in the case of PAO 4. For plain PAO 4, the COF has increased after 300 s and continued till the end of the test. This might be due to the unsteady film formation at the interfaces. A similar trend was also seen for plain PAO 100. All PAO oils exhibited the best antifriction property at an optimum concentration of 0.075 wt.% of MWCNTs, whereas PAO 40 has shown 0.025 wt.% as an optimum concentration. For all base oils with optimum additive concentration, during the initial stage of the test, there was a small increase in the COF, and there afterward, the COF decreased with the test duration. The plain PAO 40 and PAO 40+0.025 wt.% MWCNTs displayed an almost similar trend of COF with the test duration, whereas with the addition of 0.025 wt.% MWCNTs improved the antifriction performance.

It could be noticed that the COF of plain PAO 40 was around 0.059 at the beginning and stable up to 600 s; thereafter, the COF increased drastically from 0.056 to 0.086 and continuously decreased slowly till the end of the test (0.039). The PAO 40 with 0.025 wt.% MWCNTs displayed an almost similar trend of COF with test duration and exhibited the best anti-friction performance, and the final value of COF was 0.024. The remarkable increase in COF during the beginning of the test is called the running-in period. The hypothesis is that when new surfaces come in contact during the running-in condition, a more significant amount of wear is produced due to the rubbing of asperities until it establishes a stable phase, which increases the friction [132]. In the case of PAO 6 with 0.075 wt.%, the COF continuously decreased with the test duration and fluctuated between 0.064 and 0.027.

The variation in mean COF and the percentage reduction in COF with nano-additive concentration is depicted in **Figures 4.3(b) -4.3(f)**, respectively. The summary of COF, wear scar diameter (WSD), and mean wear volume (MWV) has been given in **Table 4.1**. Comparing the COF values of pure PAO 4 and PAO 4+0.075 wt.% MWCNT, which was 0.087 and 0.073, respectively, exhibited a reduction of around 20%. In the case of PAO 6 and PAO 100, the friction reduction at an optimum concentration of 0.075 wt.% of additive was about 31 and 22.5 %, respectively. PAO 40 with an optimal concentration of MWCNTs (i.e., 0.025 wt.%) displayed a 27.6 % reduction in COF compared to the plain PAO 40. Also, it was observed that increasing the concentration of the additive in PAO 40 above the optimum value leads to an increase in the COF, and it was higher than that of the plain PAO 40. This type of propensity was also noticed in the case of PAO 4 and PAO 6.

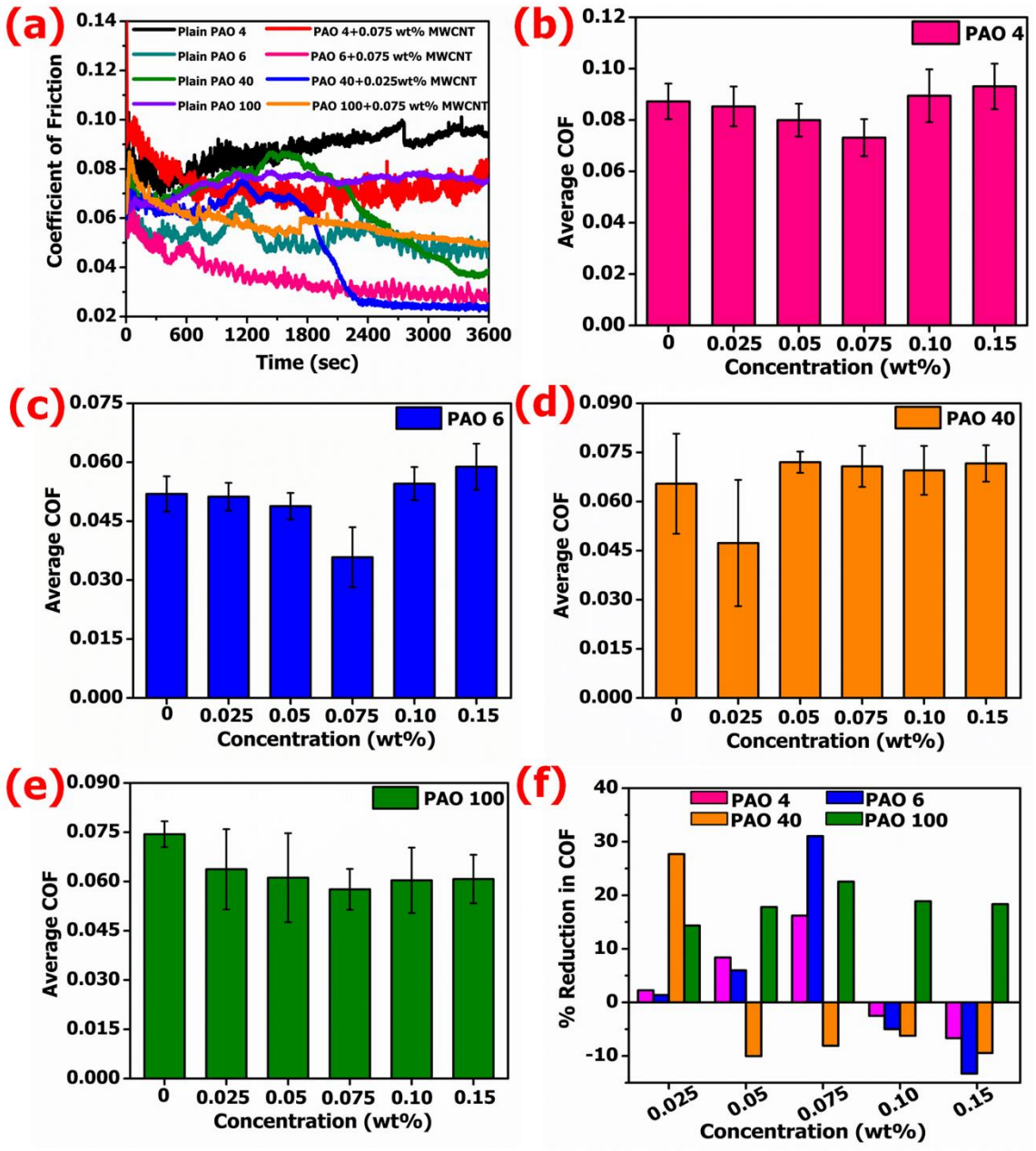

Figure 4.3: (a) Coefficient of friction as a function of test duration for various plain oil and with an optimum concentration of MWCNTs. The variation of average coefficient of friction with different concentrations of additive in (b) PAO 4 (c) PAO 6 (d) PAO 40 (e) PAO 100, and (f) percentage reduction in COF for different compositions of additive in the plain oils. (Applied load: 392 N and test duration: 60 min)

The speculation behind this phenomenon may be due to the development of large clusters because nanotubes aggregations cause three-body abrasion wear and result in higher COF [133]. **Figures 4.3(b)-4.3(e)** reveal that as the viscosity of PAO oils increases (means 4, 6, 40, and 100 as presented in **Table 3.1**), the mean value of COF at an optimum concentration of additive increases. The reason is that when the viscosities of PAOs increase, the

minimum film thickness also increases (**Eq. (C.1) of Appendix C**). The shearing action of lubricants will become difficult with an increase in the viscosity of the oil. This causes more energy requirements and increases the COF. PAO 100 highly viscous oil demonstrated a high mean COF value than PAO 6 and PAO 40 at an optimum concentration of MWCNTs.

Table 4.1: The summary of COF, WSD, and MWV for different lubricant compositions

Tribological property	**Base oil**	**MWCNTs concentration (wt.%) in PAOs**					
		0	**0.025**	**0.050**	**0.075**	**0.10**	**0.15**
Coefficient of friction (COF)	PAO 4	0.087	0.085	0.080	0.073	0.089	0.093
	PAO 6	0.052	0.051	0.049	0.036	0.055	0.059
	PAO 40	0.065	0.047	0.072	0.071	0.070	0.072
	PAO 100	0.074	0.064	0.061	0.058	0.060	0.061
Wear scar diameter, WSD (µm)	PAO 4	1069	912	954	870	966	1056
	PAO 6	799	789	815	717	814	952
	PAO 40	899	730	806	802	793	861
	PAO 100	829	812	693	683	663	711
Mean wear volume, MWV, ($\times 10^{-4} mm^3$)	PAO 4	197	103	124	85	130	188
	PAO 6	60	57	65	38	64	123
	PAO 40	97	41	62	60	58	82
	PAO 100	69	64	33	31	27	37

4.1.2.2. Anti-wear behaviour of nanolubricants

Figure 4.4 demonstrates the response of WSD, mean wear volume (MWV), and percentage reduction in WSD with increasing concentration of MWCNTs in different grades of PAO base oils. In the case of PAO 4, the WSD decreases with the addition of 0.025 wt.% of MWCNTs but further increases in the amount of additive, and there is a small increment in WSD, and nevertheless, it was lesser than that of plain PAO 4. At 0.075 wt.% of additive, the optimal WSD was noticed, and the maximum reduction was about 19%. Afterward, the WSD of steel balls continuously increases with the increase in the concentration of nanotubes. WSD of all base lubricants with varying concentrations of MWCNTs has been shown in **Table 4.1**. PAO 6 with 0.075 wt.% unveils minimum reduction in scar diameter of about 10% as compared to plain PAO 6. The WSD was reduced by around 18% in the case of PAO 40 with an optimal fraction of 0.025 wt.% of the additive. The minimum WSD and maximum reduction have been offered by PAO 100 with the best dose of 0.1 wt.% MWCNTs was about 20% compared to all admixture of additive and different grades of PAOs as illustrated in **Figures 4.4(d)** and **4.4(I)**. The MWV was calculated with the aid of WSD and the mechanical property of the steel ball [134]. The MWV of steel ball lubricated by PAO 4, PAO 6, PAO 40, and PAO 100 with an optimal fraction of additive was reduced by around 57, 36, 58, and 61%, respectively, as shown in **Figure 4.4(j)**. It can be observed from **Figures. 4.4(a)-4.4(e)** and **Table 4.1** that the WSD and MWV of plain PAO4 were too large compared to all other PAOs, but it exhibited a remarkable decrement at an optimum concentration. However, the values are still larger than other PAO oils. It may be concluded from the results that the anti-wear ability of PAOs depends not only on the concentration of additive but also on the viscosity. Along with a dose of additive, as the viscosity increases (i.e., from 4 cSt to 100 cSt), the anti-wear properties of base oils were improved. Hence, a combined effect of additive concentration and viscosity has been

recognized as an essential factor for the anti-wear ability of the base oils. On the contrary, the antifriction characteristics of lubricants worsen, as indicated in **Figure 4.3**.

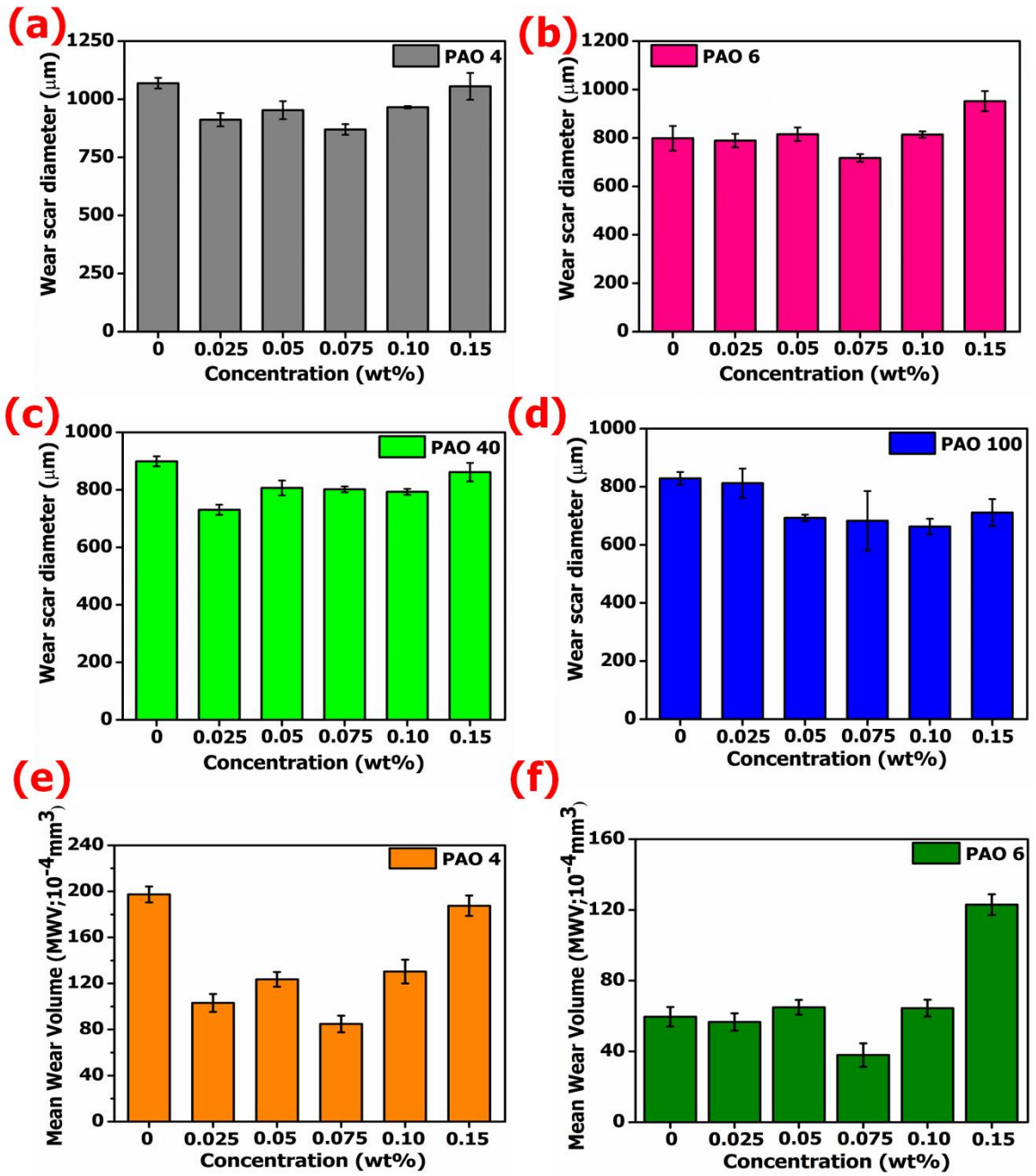

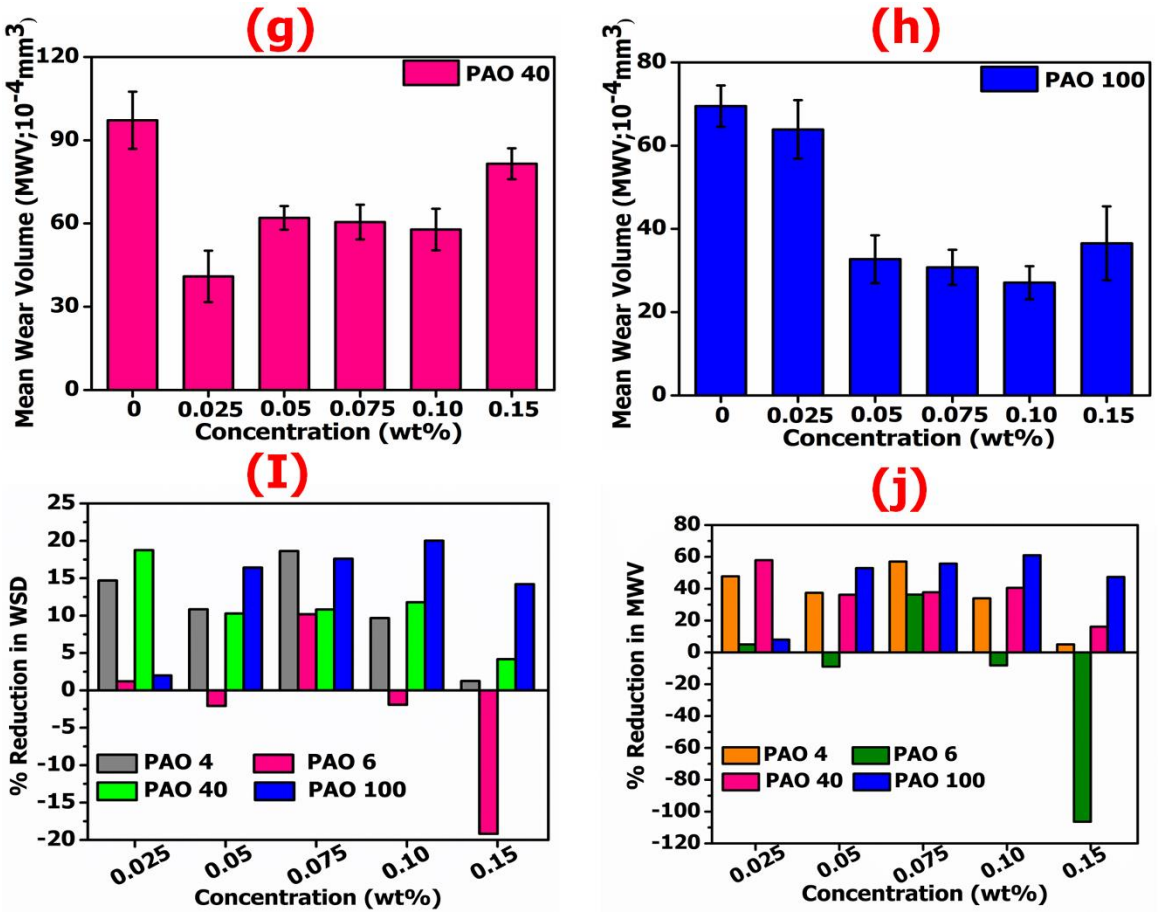

Figure 4.4: Influences of different concentrations of MWCNTs: (a)-(d) mean wear scar diameter of worn surfaces; (e)-(h) the mean wear volume; (I) the percentage reduction in WSD; and (j) MWV with different amounts of additive in PAO 4, PAO 6, PAO 40, and PAO 100. (Applied load: 392 N and test duration: 60 min)

4.1.2.3. Extreme pressure (EP) performance of nanolubricants

The EP behaviour of all PAOs base oil with varying concentrations of MWCNTs has been shown in **Table 4.2**. The EP tests revealed that steel balls get welded together due to the sudden failure of lubricant film by the application of load, which leads to heavy material removal and generation of a large amount of heat at the interface of rubbing surfaces due to metal-to-metal contact. From **Table 4.2**, it was noticed that all concentrations of MWCNTs in PAO 4 and PAO 6 were unable to influence on the EP performance. The pre-seizure and weld load for both lubricants were seen at 126 kgf and 160 kgf, respectively. For PAO 40 incorporating 0.025–0.15 wt.% concentrations of additives, test results were identical. However, improvement in load-carrying capacity was seen as compared to plain

PAO 40. Further, the pre-seizer and weld load were increased from 126 to 160 kgf and 160 to 200 kgf, respectively. Furthermore, it was observed that plain PAO 100 offered improvements in EP performance over plain PAO 4, 6, and PAO 40. The PAO 100 shows high viscosity characteristics, which contribute to form lubricant film that can sustain under high loading conditions. The dose of MWCNTs from 0.1 to 0.15 wt.% strengthened the load-carrying capacity of PAO 100. The PAO 100 with 0.1 and 0.15 wt.% MWCNTs offered the best EP performance among all PAOs based nanolubricants. The pre-seizer and weld loads were ascertained at 200 and 250 kgf, respectively. From the results of the EP test, it can be concluded that the EP performance of PAO 4 and PAO 6 was not affected greatly with the addition of MWCNTs. The higher concentration of MWCNTs, along with an increase in viscosity, as observed in the case of PAO 40 and PAO 100, improved the load-carrying capacity and EP performance.

Table 4.2: The outline of EP response of different lubricant formulations

Base lubricant	**PAO 4**		**PAO 6**		**PAO 40**		**PAO 100**	
Concentration (wt.%)	**Pre-seizer load (Kgf)**	**Weld load (Kgf)**	**Pre-seizer load (Kgf)**	**Weld load (Kgf)**	**Pre-seizer load (Kgf)**	**Weld load (Kgf)**	**Pre-seizer load (Kgf)**	**Weld load (Kgf)**
0	126	160	126	160	126	160	160	200
0.025	126	160	126	160	160	200	160	200
0.050	126	160	126	160	160	200	160	200
0.075	126	160	126	160	160	200	160	200
0.10	126	160	126	160	160	200	200	250
0.15	126	160	126	160	160	200	200	250

4.1.3. The investigation of worn surfaces

The SEM images and surfaces roughness profiles of worn surfaces of steel balls lubricated with plain PAOs and PAOs containing an optimum concentration of MWCNTs have been displayed in **Figures 4.5** and **4.6**. The deep and shallow furrow appearance along the sliding direction has been observed on the worn surfaces indicating the intensive local abrasion. The worn surface lubricated with plain PAO 4 (i.e., **Figure 4.5(a)**) has displayed a smooth and shallow groove compared to PAO 4 with 0.075 wt.% MWCNTs (**Figure 4.5(b)**). When 0.075 wt.% of MWCNTs was added in PAO 4, the hard and very brittle nature of MWCNTs caused the three-body abrasion between the metallic contacts. This resulted in the formation of tribo-film on worn surfaces by tribo chemical interaction between the functionalized MWCNTs and metal contacts or by the material transfer through stratification and exfoliation of MWCNTs over the metallic surfaces at a higher load [135–137]. This mechanism enhanced the tribological performances, and it is depicted in **Figures 4.3** and **4.4**. On the contrary, the deep grooves and adhesion of additive on the worn surfaces worsen the roughness compared to plain PAO 4, which was confirmed by the SPM micrographs (**Figures 4.6-4.7** and **Table 4.3**). The SPM micrographs (**Figures 4.6(a)-4.6(b$_1$)** represent ploughing marks and highly grooved features on the worn surface, this indicates boundary lubrication regime, and it was confirmed using **Eq. (C.1) of Appendix-C**. The average surface roughness (Sq) of the worn surface lubricated with PAO 4 of 0.075 wt.% is increased around 64% compared to plain PAO 4. The smoothest worn surface and less furrows were observed in the case of PAO 100 with 0.1 wt.% MWCNTs that is manifested by SEM images (**Figure 4.5**), and it was also justified by SPM results. The SPM results demonstrate that the average surface roughness of the worn surface of steel balls experimented with plain PAO 100 decreased significantly when 0.1 wt.% MWCNTs was added in PAO 100 and exhibited a remarkable reduction (approximately 57%). The values

of the surface roughness of plain PAOs and PAOs with an optimum concentration of additive are listed in **Table 4.3**. The highly viscous characteristics of PAO 100 helped to form a mixed or partial lubrication regime (λ= 1.18), and this caused the separation of the mating surfaces and enhanced the tribological performance via various hypothesis mechanisms like mending, rolling, polishing effect, and formation of protective tribo film as discussed by many researchers [65–67]. The proposed lubrication mechanism and role of MWCNTs on the tribological performance have been discussed in the later part of the discussion (Section. 4.1.4). A 2D contact-type profilometer was also employed to measure the depth of wear scar of steel balls lubricated with various lubricant compositions. **Figure 4.7** represents the linear profile curve of wear scar, and **Table 4.4** shows the typical values for different PAO-based nanolubricants. The maximum height difference (i.e., depth) of wear scar was observed in the case of plain PAO 4 (20.1 µm) and found to be the highest MWV among all the nanolubricants tested, and it is shown in **Figure 4.4**. But there was an improvement in depth (12.5 µm) when 0.075 wt.% of MWCNTs were doped in PAO 4. However, 0.075 wt.% doses of additive in PAO 4 have worsened the worn surface's roughness, which was affirmed by the SPM analysis (**Figure 4.6**). It was also noticed that as the viscosity of lubricants increases (i.e., from PAO 6 to PAO 100), and with the addition of an optimum dose of MWCNTs in PAOs, the anti-wear performances, as well as surface topography of worn surfaces, improved significantly as illustrated by SEM, SPM and profilometer results (**Figures 4.5-4.7**).

The EDS has been carried out to probe the element identification and contribution of MWCNTs in the formation of tribo film on the contacting metal surfaces. **Figure 4.8** shows the EDS spectrum and weight % and atomic % of individual elements of selected worn surfaces of steel balls tested with different grades of plain PAOs and with an optimum dose of additive. The iron peak in all micrographs in **Figure 4.8** represents the uniform

distribution of iron. It is a significant ingredient of steel balls and has a measurable presence of carbon and chromium. It is shown in Figures **4.8(b$_1$)-4.8(h$_1$)** that the admixture of MWCNTs in PAOs has increased the peak, weight % as well as atomic% of carbon element and evident for the formation of thin tribo-film. The absence of O peak indicates that MWCNTs did not seem to be oxidized to any significant extent [138].

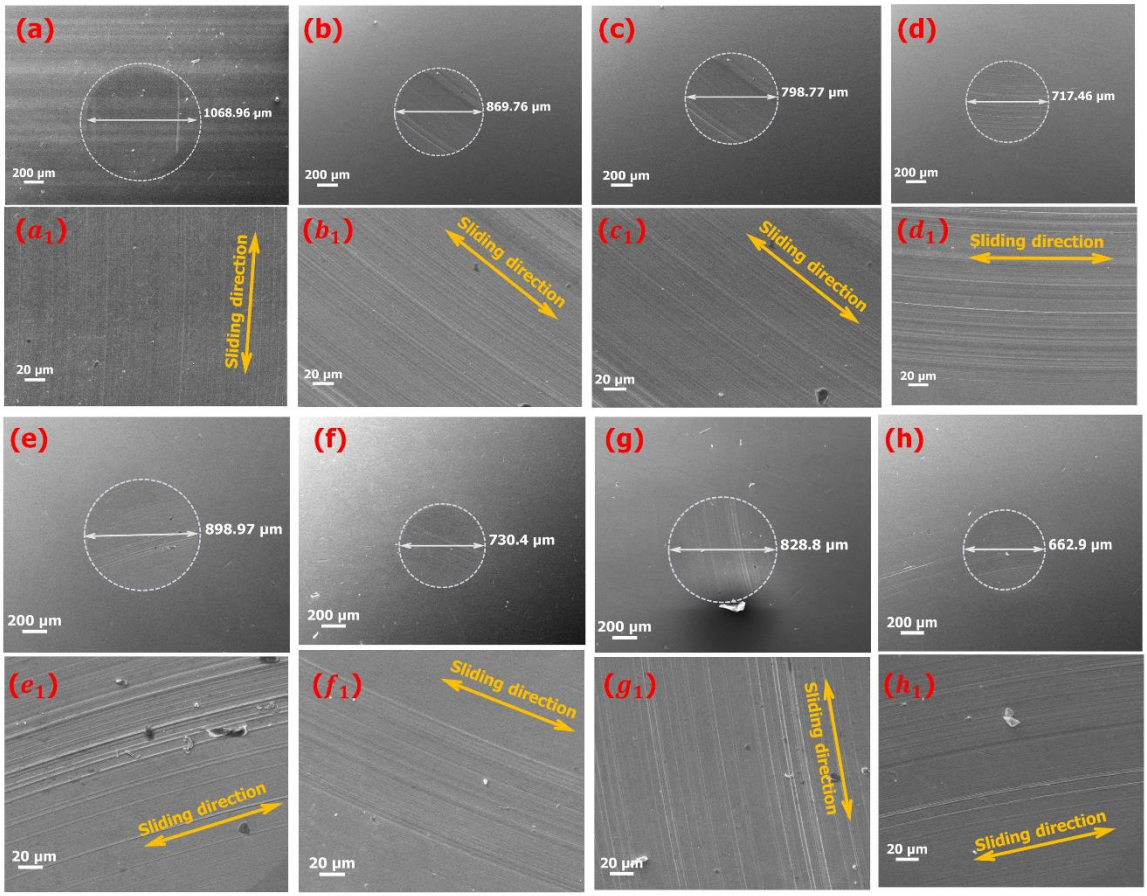

Figure 4.5: The SEM micrographs of wear scars of steel balls lubricated with (a, a1) plain PAO4; (b, b$_1$) PAO 4 with 0.075 wt.% MWCNTs; (c, c$_1$) plain PAO 6; (d, d$_1$) PAO 6 with 0.075 wt.% MWCNTs; (e, e$_1$) plain PAO 40; (f, f$_1$) PAO 40 with 0.025 wt.% MWCNTs; (g, g$_1$) plain PAO 100; (h, h$_1$) PAO 100 with 0.1 wt.% MWCNTs. [Note: - a, b, c, d, e, f, g, h: at 100X; and a$_1$, b$_1$, c$_1$, d$_1$, e$_1$, f$_1$, g$_1$, h$_1$: at 2000X]. (Applied load: 392 N and test duration: 60 min)

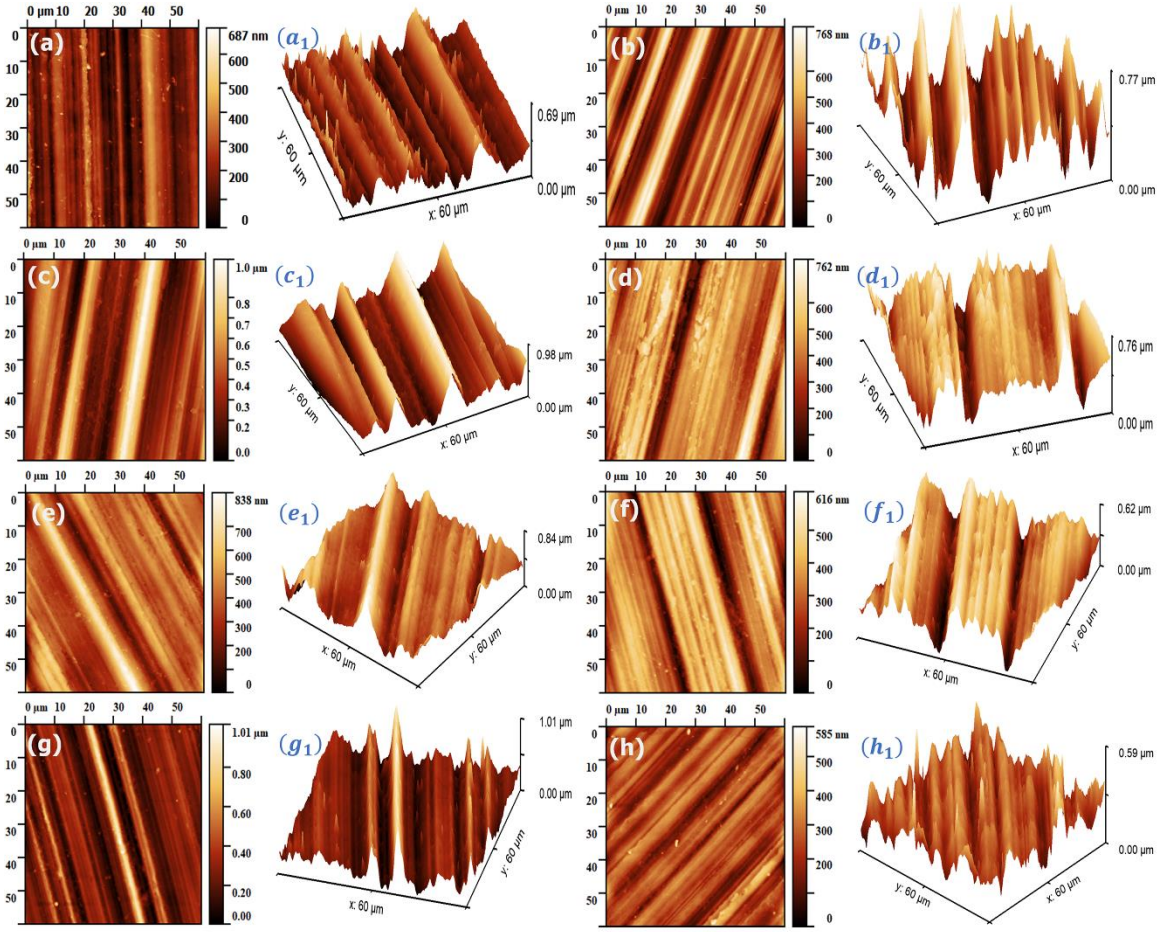

Figure 4.6: SPM roughness images of worn surfaces of steel balls, (a, a_1) plain PAO 4; (b, b_1) PAO 4 with 0.075 wt.% MWCNTs; (c, c_1) plain PAO 6; (d, d_1) PAO 6 with 0.075 wt.% MWCNTs; (e, e_1) plain PAO 40; (f, f_1) PAO 40 with 0.025 wt.% MWCNTs; (g, g_1) plain PAO 100; (h, h_1) PAO 100 with 0.1 wt.% MWCNTs. [Note: - a, b, c, d, e, f, g, h: 2D view and a_1, b_1, c_1, d_1, e_1, f_1, g_1, h_1: 3 D view of worn surfaces]. (Applied load: 392 N and test duration: 60 min)

Table 4.5 describes the compatibility of MWCNTs with different PAO oils. Both enhanced and degraded tribological properties were observed in PAOs-based nanolubricants at sliding contact. In this present investigation, the results of tribo testing unveiled the good compatibility of MWCNTs with PAO 40 and PAO 100 but moderate compatibility with PAO 4 and PAO 6. It was presumed that higher viscous characteristics of PAO oils are responsible for better suspension of additive in a liquid medium because PAO 40 and PAO 100 are more viscous than PAO 4 and PAO 6. **Figure 4.9** illustrates the outcomes of tribological testing and the effect of the addition of MWCNTs on the tribological properties of the PAO oils.

Table 4.3: The summary of surface roughness of worn steel balls tested with various lubricant compositions

Samples	Surface roughness	
	S_a (nm)	S_q (nm)
PAO 4	76.678	93.965
PAO 4 +0.075 wt.% MWCNTs	125.086	153.970
PAO 6	163.719	198.838
PAO 6 +0.075 wt.% MWCNTs	99.750	128.761
PAO 40	95.149	122.632
PAO 40 +0.025 wt.% MWCNTs	94.970	119.213
PAO 100	109.548	151.107
PAO 100 +0.1 wt.% MWCNTs	53.299	65.443

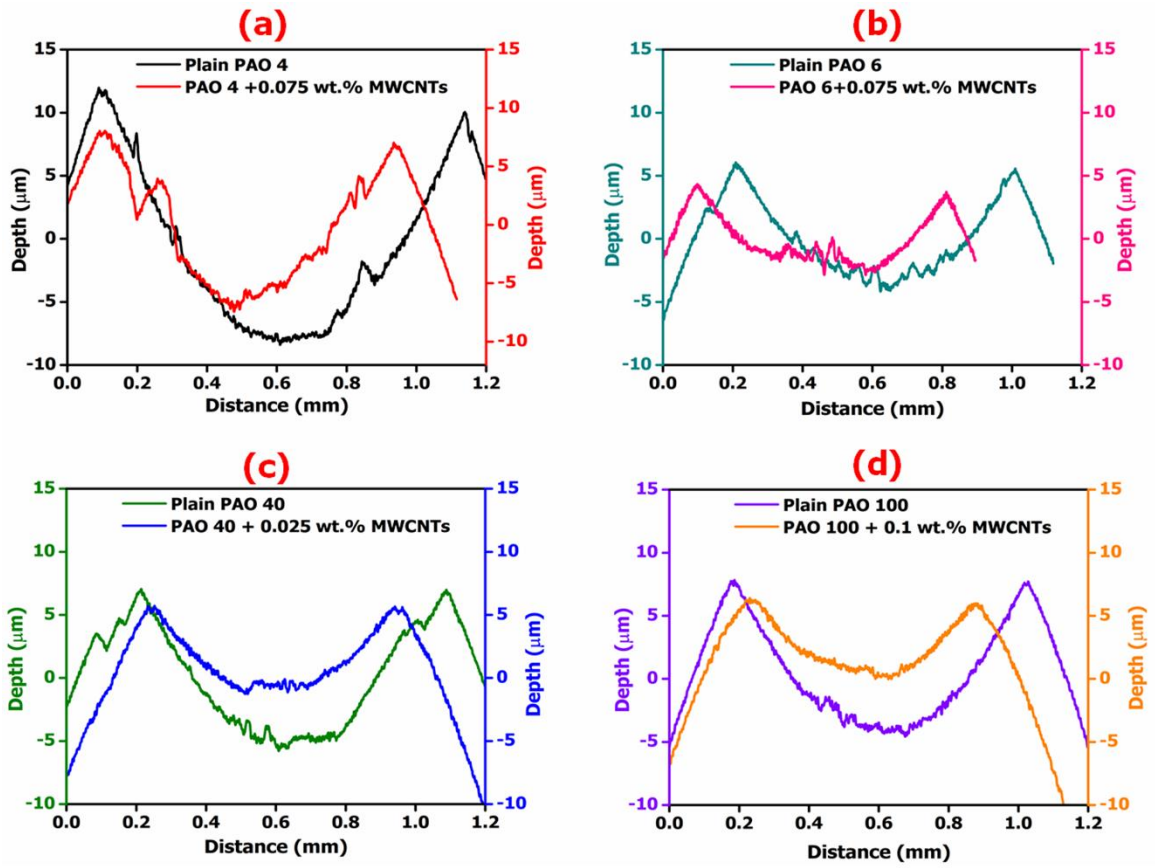

Figure 4.7: Linear roughness profile of worn surfaces measured in the 2D contact profilometer. (Applied load: 392 N and test duration: 60 min)

Table 4.4: The summary of typical values of worn surfaces for the various composition of nanolubricants

Sample details	Line roughness		Height difference (i.e., depth) (μm)	Horizontal distance (i.e., diameter) (μm)
	R_a (μm)	R_q (μm)		
PAO 4	0.475	0.562	20.1	1050
PAO 4 +0.075 wt.% MWCNTs	0.639	0.769	12.5	854
PAO 6	0.396	0.493	10.1	798
PAO 6 +0.075 wt.% MWCNTs	0.307	0.408	7	718
PAO 40	0.404	0.535	12.4	881
PAO 40 +0.025 wt.% MWCNTs	0.331	0.405	6.74	731
PAO 100	0.442	0.564	11.7	841
PAO 100 +0.1 wt.% MWCNTs	0.333	0.389	5.26	658

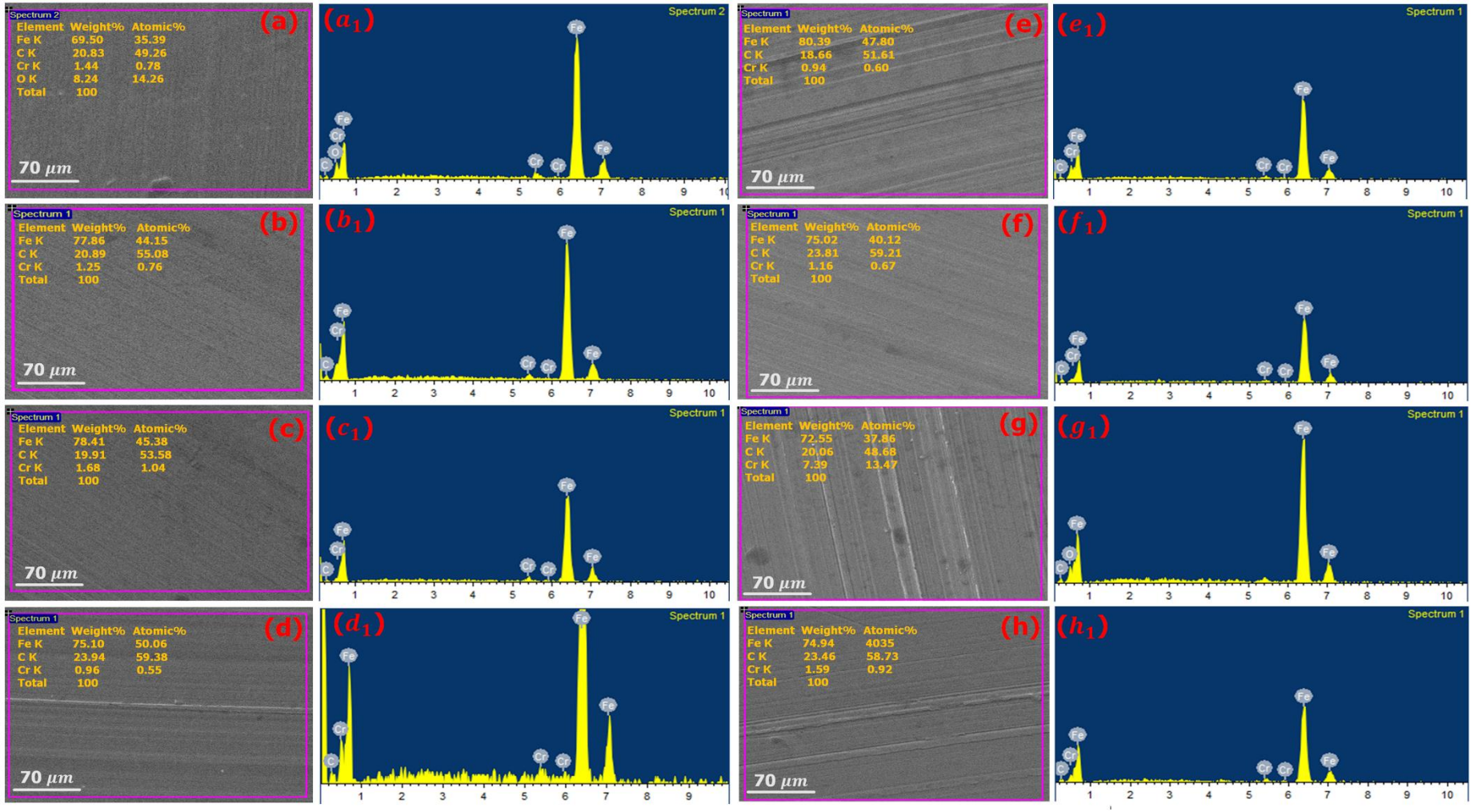

Figure 4.8: The EDS spectra of wear scars of steel balls tested with (a, a_1) plain PAO 4; (b, b_1) PAO 4 with 0.075 wt.% MWCNTs; (c, c_1) plain PAO 6; (d, d_1) PAO 6 with 0.075 wt.% MWCNTs; (e, e_1) plain PAO 40; (f, f_1) PAO 40 with 0.025 wt.% MWCNTs; (g, g_1) plain PAO 100; and (h) and (h_1), PAO 100 with 0.1 wt.% MWCNTs. (Applied load: 392 N and test duration: 60 min)

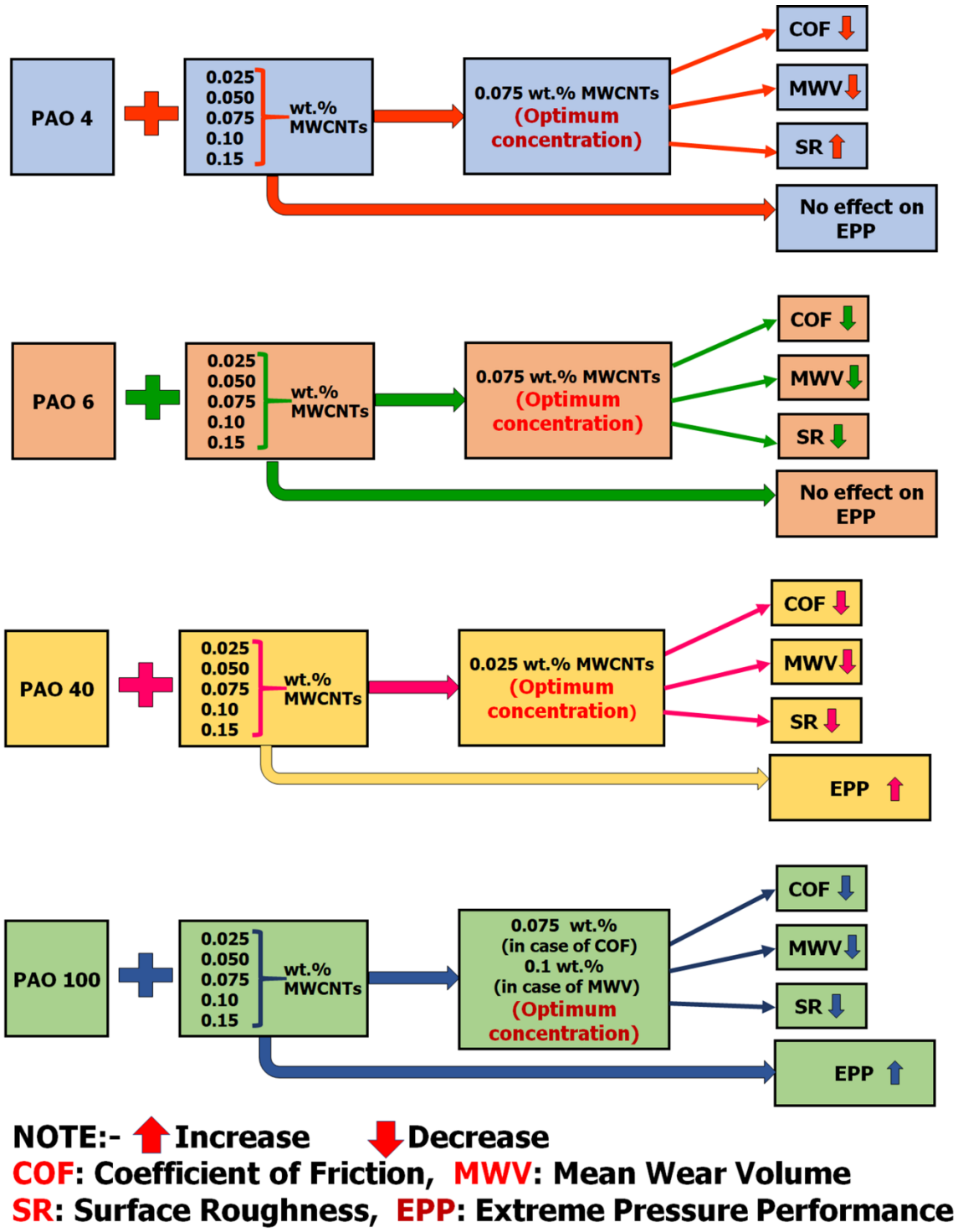

Figure 4.9: The flowchart represents the influences of MWCNTs on the tribological performance of different PAO oils

Table 4.5: The summary of MWCNTs compatibility with different grades of PAO oils

Nanolubricants	Compatible		Compatibility Potency	COF	MWV
	Yes	No			
PAO 4+0.025 wt.% MWCNTs	✗	✓	Low	↓	↓
PAO 4+0.05 wt.% MWCNTs	✗	✓	Low	↓	↓
PAO 4+0.075 wt.% MWCNTs	✓	✗	Moderate	↓	↓
PAO 4+0.1 wt.% MWCNTs	✓	✗	Moderate	↑	↓
PAO 4+0.15 wt.% MWCNTs	✓	✗	Moderate	↑	↓
PAO 6+0.025 wt.% MWCNTs	✗	✓	Low	↓	↓
PAO 6+0.05 wt.% MWCNTs	✓	✗	Moderate	↓	↑
PAO 6+0.075 wt.% MWCNTs	✓	✗	Moderate	↓	↓
PAO 6+0.10 wt.% MWCNTs	✓	✗	high	↑	↑

PAO 6+0.15 wt.% MWCNTs	✓	✗	High	↑	↑
PAO 40+0.025 wt.% MWCNTs	✓	✗	High	↓	↓
PAO 40+0.050 wt.% MWCNTs	✓	✗	High	↑	↓
PAO 40+0.075 wt.% MWCNTs	✓	✗	High	↑	↓
PAO 40+0.10 wt.% MWCNTs	✓	✗	High	↑	↓
PAO 40+0.15 wt.% MWCNTs	✓	✗	high	↑	↓
PAO 100+0.025 wt.% MWCNTs	✓	✗	High	↓	↓
PAO 100+0.05 wt.% MWCNTs	✓	✗	High	↓	↓
PAO 100+0.075 wt.% MWCNTs	✓	✗	High	↓	↓
PAO 100+0.1 wt.% MWCNTs	✓	✗	High	↓	↓
PAO 100+0.15 wt.% MWCNTs	✓	✗	High	↓	↓

4.1.4. Proposed lubrication mechanism

The proposed lubrication mechanism with MWCNTs on the tribological performance has been demonstrated with the schematic diagram (**Figure 4.10**). The MWCNTs that enter into the grooves or asperity of the mating surfaces and easily roll between the friction pair called the bearing effect. If it is deposited on the valleys of the mating surfaces featuring mending effect. This facilitates the distribution of pressure over the large contact area. Hence, the wear of steel balls decreases. It can also be speculated that some MWCNTs can exfoliate at higher loads and behave like lamellar nanosheets. These nanosheets adhere to the rubbing surfaces that form a transfer layer onto the surfaces of the tribological pair and produce a low-energy surface, contributing to lowering the friction and wear.

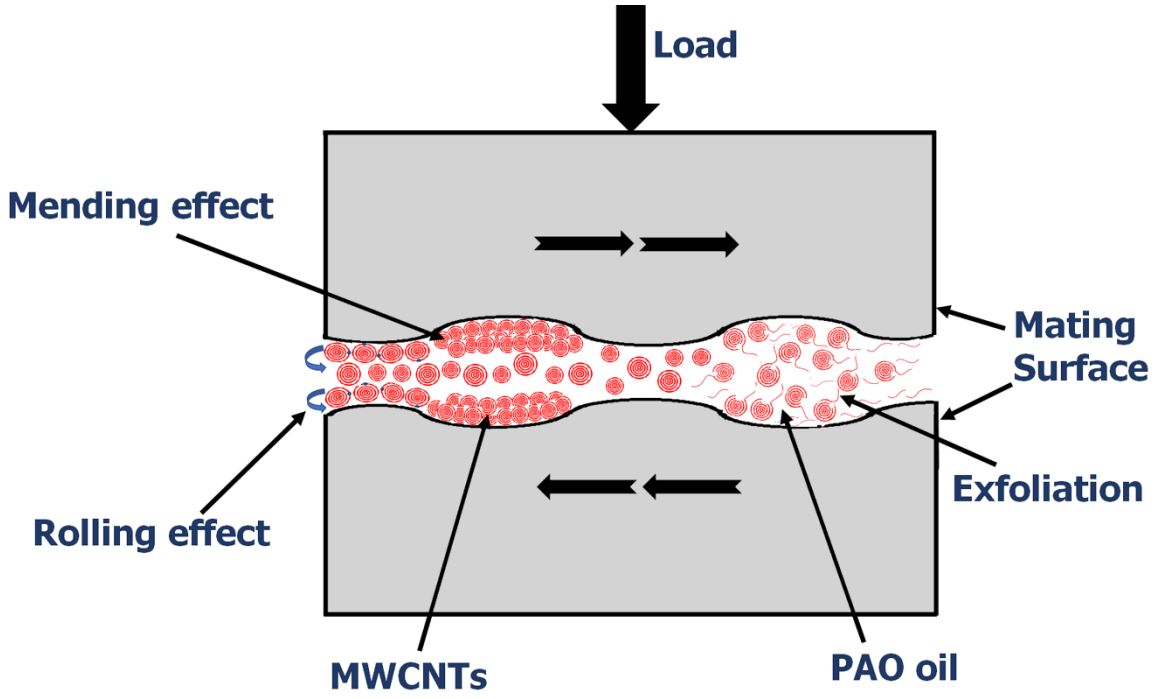

Figure 4.10: Schematic diagram demonstrates the lubrication mechanism and role of MWCNTs.

4.2. Part-B: Tribological investigation of PAOs-based and PPG based nanolubricants under starved lubrication conditions using SRV 5 tribo-test rig

4.2.1. Tribological evaluation of high viscosity synthetic base oils (PAO 100 and PPG 2000) based nanolubricants

4.2.1.1. Friction and wear response of nanolubricants

4.2.1.1.1. Friction performance of nanolubricants

The variation in the average coefficient of friction (COF) and percentage attenuation with additive concentration for both base oils is shown in **Figures 4.11(a)** and **4.11(b)**. The results demonstrated that incorporating a small amount of additive in the base oils enhances COF to a significant level. In both nanolubricants, minimum COF was achieved at 0.025 wt.% doses of the additive, and increasing additive concentration in both base oils above 0.025 wt.% leads to an increase in COF. Still, it remains lower than that of plain oil for PAO 100. In the case of PPG 2000 beyond 0.025 wt.% of MWCNTs, the increase in COF was higher relative to the base oil. This outcome may be caused by the aggregation of bundles of nanotubes, which initiates for three-body abrasion wear, and it could be the reason for higher COF. At a concentration of 0.025 wt.% of additive, the average COF for PAO 100 and PPG 2000 was 0.125 and 0.206, respectively, and the maximum reduction in COF was 12 and 6%, respectively.

The variation of COF with time at a concentration of 0.025 wt.% of MWCNTs as an additive in PAO 100 and PPG 2000 is presented in **Figure 4.11(c)**. For plain PAO 100, at the initial stage of the test, there was an increase in the COF, and subsequently, the variation of COF was almost independent of time. The rise in coefficient of friction at the initial stage

may be due to the absence of film formation at the interface of mating pairs, which leads to severe wear of surfaces and an increase in friction. The same trend is also seen for PAO 100 with 0.025 wt.% of the additive. While comparing the plain PAO 100 with plain PPG 2000, it was observed that there was a small difference in the COF during the initial run, but it kept increasing with time. This difference in the COF between these oils was larger with time as the test progressed. This phenomenon was also observed while comparing PAO 100 and PPG 2000, containing 0.025 wt.% of MWCNTs. It was also noticed that by introducing a dose of 0.025 wt.% of additive in PAO 100, COF was stable throughout the test duration. The reason is that nanolubricant at the contact region (i.e., PAO 100 containing 0.025 wt.% of MWCNTs) rearrange themselves during sliding, thereby preserving excellent lubricating property for a longer duration. In the case of PPG 2000 with 0.025 wt.% MWCNTs, the COF continuously increased with time, and at the end of the test, it was slightly lower than that of plain PPG 2000.

4.2.1.1.2. Wear performance of nanolubricants

Figures 4.11(d) and **4.11(e)** demonstrate the wear volume (WV) of ball and disc specimen and percentage reduction in WV as a function of varying concentrations of MWCNTs for both base oils. The WV was estimated as the sum of WV produced in both mating surfaces. For PAO 100, the WV continuously decreased with an increase in the amount of additive up to 0.05 wt.%. But there was a sudden spurt in wear at a concentration of 0.075 wt.%, which was higher than plain PAO 100. This is because when the quantity of additive is small (0.05 wt.%) in PAO 100, the diminutive size and tubular shape of MWCNTs have an easy entrance between the mating pairs and which easily rolls and leads to a decrease in friction as well as wear. In contrast, an increasing amount of nanoadditive beyond concentration 0.05 wt.% in PAO 100 has caused a process of fluid film build-up and collapse due to agglomeration of MWCNTs followed by the three-body abrasion, which

results in diminishing the rolling capability of MWCNTs, thereby increasing the wear of the mating bodies as well as increasing friction (as displayed in **Figure 4.11(a)**). It was concluded from **Figure 4.11(d)** that the variation of wear volume for PPG 2000 (as projected on the secondary Y-axis) is higher as compared to PAO 100. In PAO 100, the minimum wear volume (i.e., 6.28×10^{-3} mm^3) was observed at 0.05 wt.% of MWCNTs, whereas for PPG 2000, it was observed at 0.025 wt.% of MWCNTs (i.e., 109.42×10^{-3} mm^3). The test results showed that a higher reduction in wear volume of around 87% was achieved in the case of PPG 2000 with 0.025 wt.% of MWCNTs compared to the plain PPG 2000. However, at all concentrations of MWCNTs in PAO 100, an excellent reduction in wear volume was observed compared to PPG 2000-based nanolubricant.

4.2.1.2. Analysis of worn surfaces

4.2.1.2.1. Analysis of worn surface of steel balls

To probe the anti-wear mechanism of COOH-functionalized MWCNTs, the test balls lubricated with plain base oils and oils containing MWCNTs were investigated using SEM and SPM are presented in **Figures 4.12** and **4.13**. The worn surface lubricated by plain PPG 2000 in **Figures 4.12(a)** and **4.12(a_1)** revealed a more prominent scar with deep furrows, large pits, and considerable wear debris along the sliding direction. It can be anticipated that due to the continuous sliding of friction pairs, the lubricant is unable to preserve the tribo-film because the quantity of lubricant used was 0.3 ml, which leads to the occurrence of surface-originated spalling. Adhesive wear and abrasive wear are identified as the prime mode of wear. The worn surface of PPG 2000 containing concentration 0.025 wt.% of MWCNTs, presented in **Figures 4.12(b)** and **4.12(b_1)**, also showed a more significant wear scar but smaller than plain PPG 2000 with relatively sleek rubbing marks, which demonstrated that furrows were alleviated due to the addition of MWCNTs.

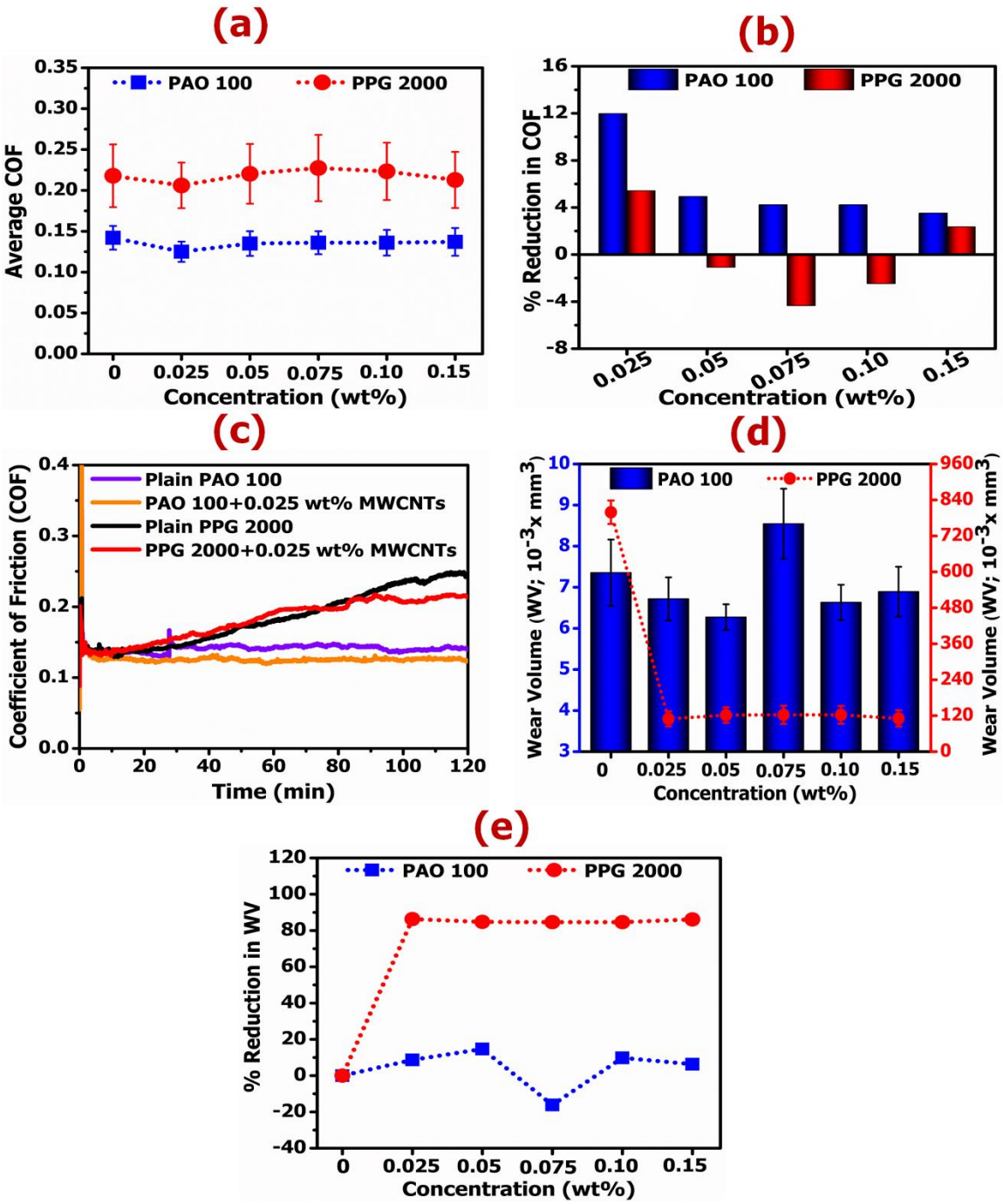

Figure 4.11: Variation of coefficient of friction (a) with different concentrations of additive in PAO 100, PPG 2000, (b) percentage reduction in COF (c) with test duration, (d) the variation of wear volume with different compositions of additive in both base oils, and (e) percentage reduction in WV. (Applied load: 300 N and test duration: 120 min)

However, the wear scar of steel ball lubricated with plain PAO 100 is smaller (**Figure 4.12(c)**) than the plain PPG 2000 and PPG 2000 with 0.025 wt.% of the additive. PAO 100 exhibited better characteristics (higher viscosity and higher VI) than PPG 2000, exhibiting a mixed or partial lubrication regime. In contrast, a boundary lubrication process was

observed in the case of PPG 2000, calculated using **Eq. (C.1) of Appendix-C**. This mixed lubrication regime caused the separation of the mating surfaces and enhanced tribological performance. The anti-wear property of PAO 100 was further enhanced with the inclusion of 0.05 wt.% of additive, as shown in **Figures 4.12(d)- 4.12(d_1)**. The enlarged view (at higher magnification) of the wear scar for plain PAO 100 (**Figure 4.12(c_1)**) clearly shows the deep furrow and micro pit along the direction of sliding. Further, the worn surface demonstrated the presence of MWCNTs (**Figure 4.12(d_1)**) and light furrows, which implied better friction surfaces.

The SPM technique also confirmed the SEM results mentioned earlier. The SPM images and corresponding roughness values of the worn surfaces of steel balls for different lubrication compositions are shown in **Figure 4.13** and **Table 4.6**. Plain PPG 2000 (**Figures 4.13(a)-4.13(a_1)**) revealed the ploughing marks and deeply grooved features on the worn surface, while the less furrows and comparably smooth surface was observed when MWCNTs were added to PPG 2000 (**Figures 4.13(b)-4.13(b_1)**). The height of asperity in 3D view of worn surface lubricated with PPG 2000 with 0.025 wt.% of MWCNTs is higher than that of plain PPG 2000. The peeling pit, evident in the left corner of the 2 D image (**Figure. 4.13(b)**), is responsible for the increase in the height of asperity, and this type of pit is also clearly visible in **Figure 4.12(b)**. Apart from this single asperity, the worn surface seems to be smoother. The surface roughness (Sq) of worn surface lubricated with plain PPG 2000 and plain PAO 100 are 375 and 283 nm, respectively, whereas for the scar related to 0.025 wt.% MWCNTs in PPG 2000 and 0.05 wt.% in PAO 100, the surface roughness was decreased to 305 and 225.51 nm, respectively. From the above discussion, it is apparent that incorporating additives could improve the anti-wear response of both base oils.

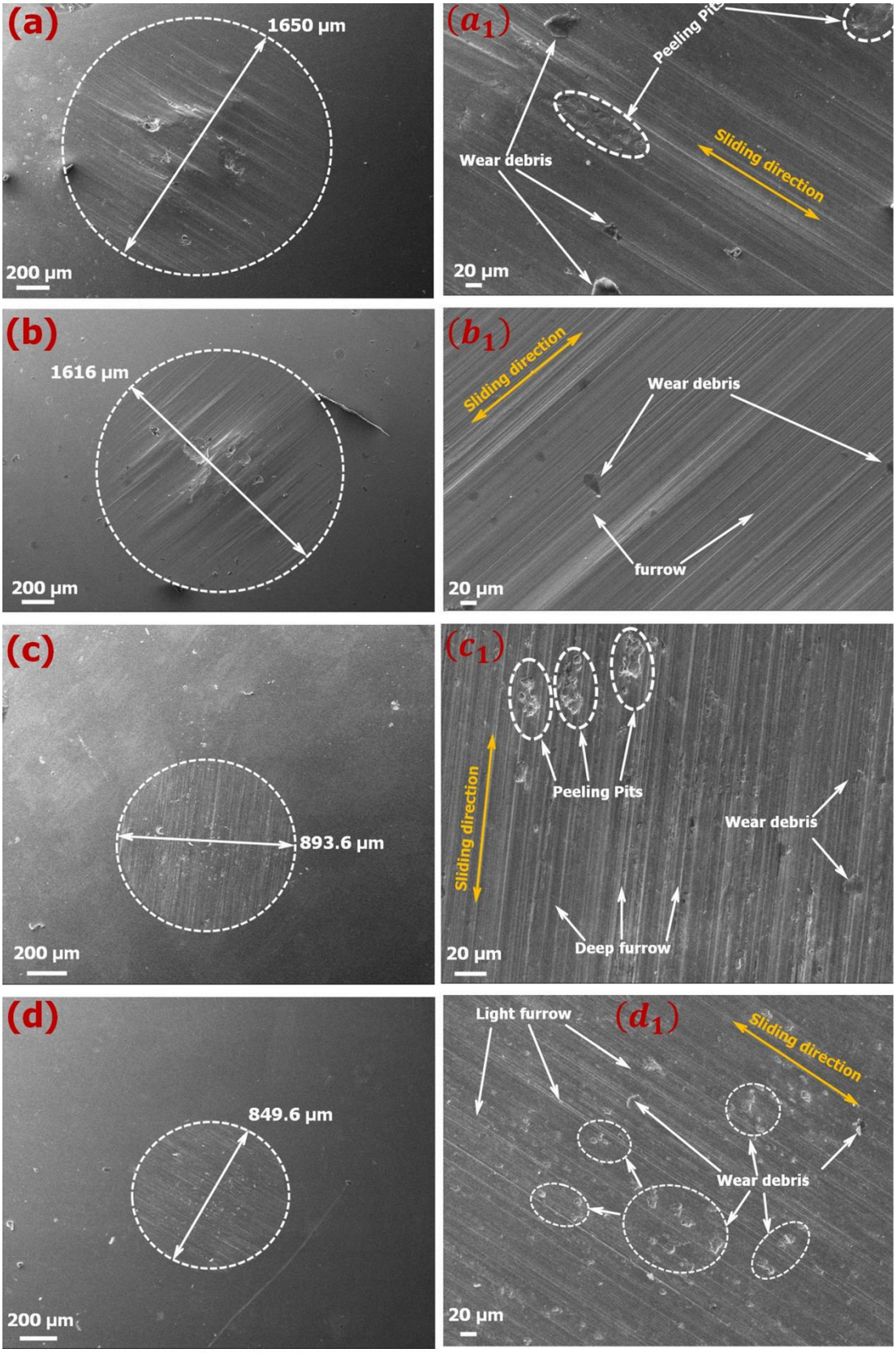

Figure 4.12: SEM micrographs of wear scars of steel balls lubricated by (a, a_1) plain PPG 2000; (b, b_1) PPG 2000 with 0.025 wt.% MWCNTs; (c, c_1) plain PAO 100, and (d, d_1) PAO 100 with 0.05 wt.% MWCNTs [Note: - a, b, c, d: at 100X; and a_1, b_1, c_1, d_1: at 1000X]. (Applied load: 300 N and test duration: 120 min)

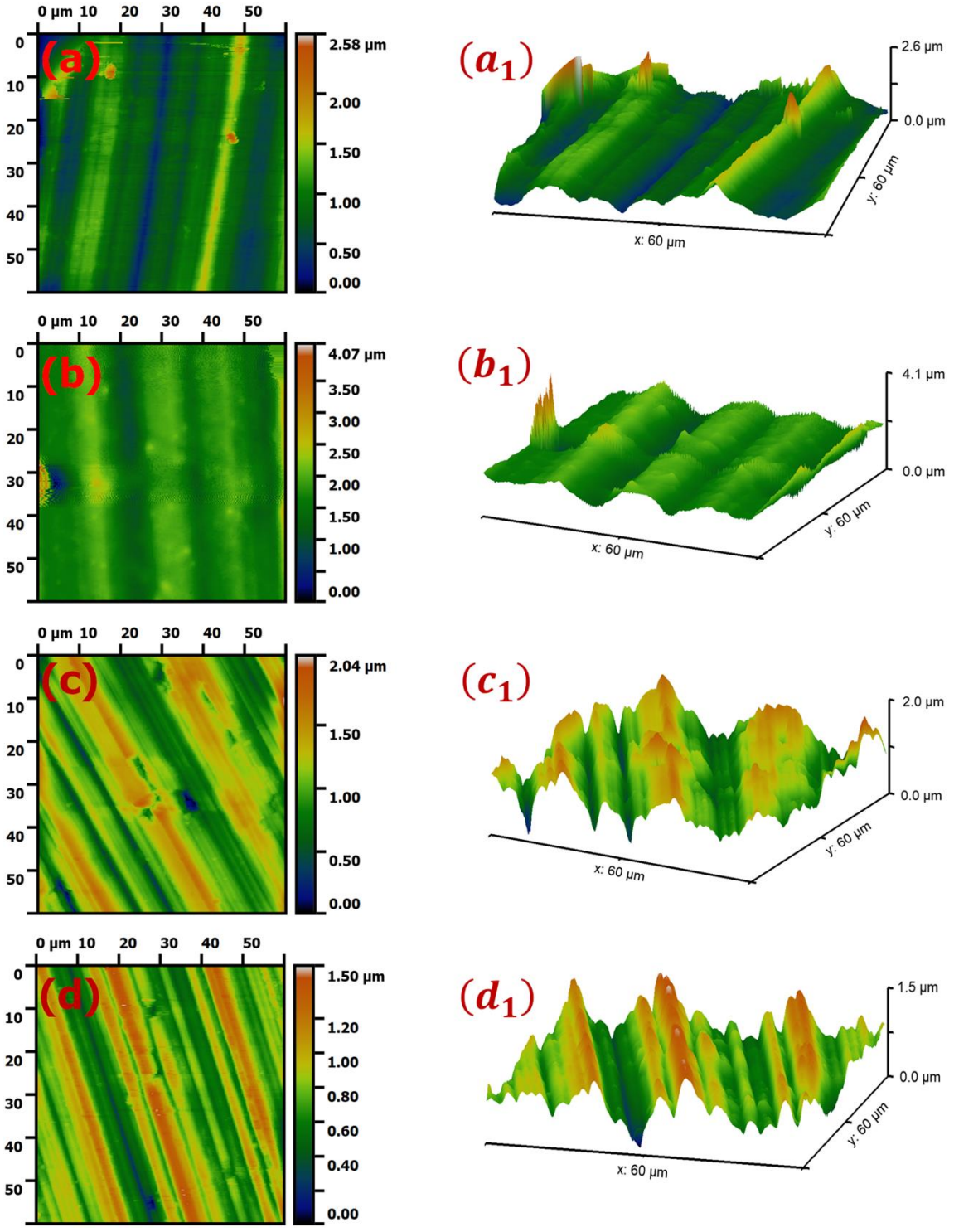

Figure 4.13: SPM pictures of worn surfaces of steel balls experimented with (a, a_1) plain PPG 2000; (b, b_1) PPG 2000 with 0.025 wt.% MWCNTs; (c, c_1) plain PAO 100, and (d, d_1) PAO 100 with 0.05 wt.% MWCNTs [Note: - a, b, c, d: Top view and a_1, b_1, c_1, d_1: Three-dimensional view of worn surfaces]. (Applied load: 300 N and test duration: 120 min)

Table 4.6: The summary of surface roughness of worn steel balls tested with various lubricant formulations

Samples	Line roughness		Surface roughness	
	R_a (nm)	R_q (nm)	S_a (nm)	S_q (nm)
PPG 2000	236	286	293	375
PPG 2000+0.025 wt.% MWCNTs	345	447	235	305
PAO 100	206	271	232	283
PAO 100 +0.05 wt.% MWCNTs	202	245	183.78	225.51

4.2.1.2.2. Worn surface analysis of disc.

The counterpart (i.e., disc) of the "ball on disc" configuration of tribo-testing was also analysed by SEM to understand the role of nanoadditive in the anti-wear performance of both types of base oils. The wear scar on the disc was examined for width, depth, and also cross-section area of the worn surface**. Figure 4.14** shows the SEM images of worn disc lubricated by plain base oils and base oils incorporating MWCNTs. The corresponding cross-section profiles of wear track and typical values of various characteristics of the worn surface are presented in **Figure 4.15** and **Table 4.7**, respectively. It can be seen from **Figures 4.14(a)-4.14(a$_1$)** that the width of the wear track on the disc lubricated by plain PPG 2000 is 1612 µm, which revealed a sign of severe scuffing. The wear surface is covered with grinding marks, many furrows with some pits, and some amount of residual wear debris. The wear surface along the direction of movement exhibited adhesion features, and the occurrence of ploughing resulted in higher friction and wear behaviour of plain PPG 2000 (**Figure 4.11**). The depth of wear track for plain PPG 2000 varies between – 3.06 and – 64.84 µm with an average depth of 63.2 µm, and the corresponding cross-section

area was 36,136 μm^2 (**Figure 4.15(a)** and **Table 4.7**). It can be seen from **Figures 4.14(b)-4.14(b$_1$)** that the wear track width decreased to 1557 μm, and a wide furrow with a relatively smoother surface was observed when 0.025 wt.% MWCNTs was added in PPG 2000. Consequently, the worn surfaces' average depth and cross-section area also decreased to 61.8 μm and 33,264 μm^2, respectively (**Figure 4.15(a)** and **Table 4.7**). For plain PAO 100, the track width, average depth, and cross-section area of the worn surface of the disc are approximately 844.6 μm, 6.8 μm, and 1873 μm^2, respectively, as shown in **Figure 4.15(b)** and **Table 4.7**. For 0.05 wt.% MWCNTs added in PAO 100, the track width, depth, and cross-section area were appreciably reduced, and their values are around 809.8 μm, 5.2 μm (~24 % reduction), and 1212 μm^2 (~36 % reduction), respectively, which is also corroborated by SEM results of the worn disc (**Figures 4.14(c)-4.14(d)**).

4.2.1.2.3. EDS analysis of worn surfaces

The EDS was carried out to ascertain the elemental composition and contribution of MWCNTs in the formation of tribo-film on the contacting surfaces. **Figure 4.16** represents the EDS spectrum along with weight % and atomic % of individual elements of the selected worn surfaces of steel balls. The EDS results of the worn surface of the disc (**Figure 4.14**) are summarized in **Table 4.8**. It was observed from **Figure 4.16** and **Table 4.8** that the EDS spectra reveal the presence of Fe, C, Cr, and O in all the worn surfaces. Fe, C, and Cr are from the steel ball and disc since these are the main constituents of test specimens, but the presence of C on the worn surface arises due to the concentration of MWCNTs or the base oil. The existence of O reveals the development of the oxide layer between the rubbing surface when the iron is exposed to air. The surfaces lubricated by plain PPG 2000 (**Figure 4.16** and **Table 4.8**) displayed a higher oxygen content among all the worn surfaces confirming an iron oxide layer formation. This type of oxide formation is the simplest form of the hindrance of wear, but the breakdown of these oxide layers may quickly occur even

at light load, which results in severe wear of friction pairs, as shown in **Figures 4.12(a)-4.12(a_1)** and **4.14(a)-4.14(a_1)**.

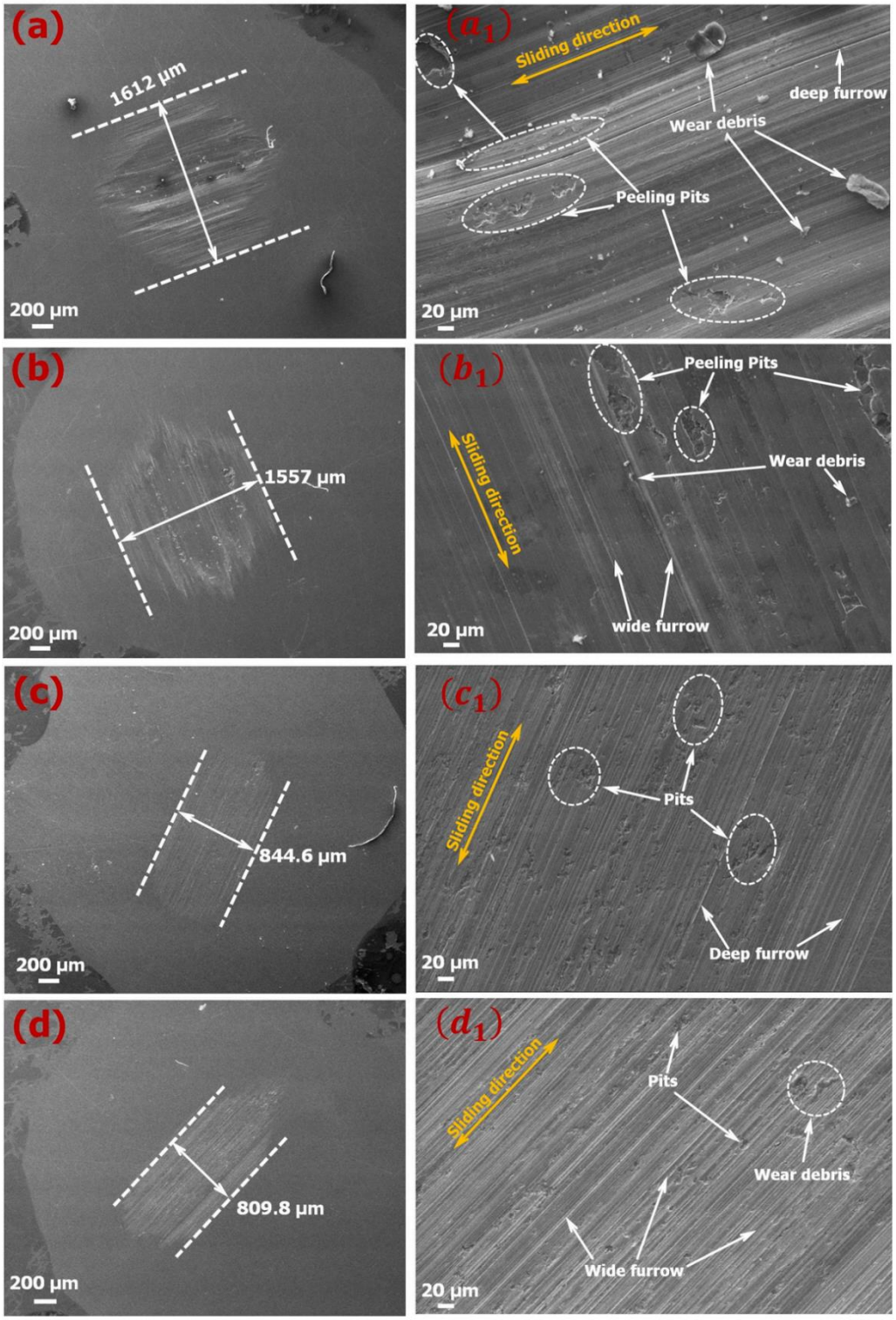

Figure 4.14: SEM images of wear scar of the steel disc after friction test (a, a_1) plain PPG 2000; (b, b_1) PPG 2000 with 0.025 wt.% MWCNTs; (c, c_1) plain PAO 100, and (d, d_1) PAO 100 with 0.05 wt.% MWCNTs [Note: - a, b, c, d: at 100X; and a_1, b_1, c_1, d_1: at 500X] (Applied load: 300 N and test duration: 120 min)

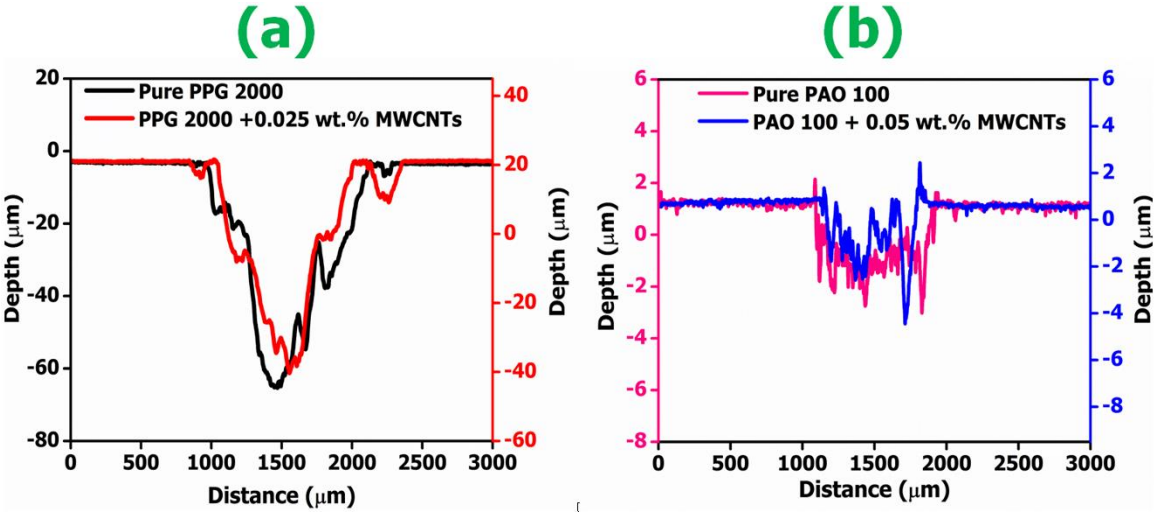

Figure 4.15: The cross-section profile of wear track of the disc lubricated with (a) plain PPG 2000 and PPG 2000 with 0.025 wt.% MWCNTs, and (b) plain PAO 100 and PAO 100 with 0.05 wt.% MWCNTs. (Applied load: 300 N and test duration: 120 min)

Table 4.7: The summary of the various characteristics of worn steel disc tested with different lubricants

Samples	Wear track width, (μm)	Wear track depth, (μm)	Cross-section area, (μm^2)
PPG 2000	1612	63.2	36136
PPG 2000+0.025 wt.% MWCNTs	1557	61.8	33264
PAO 100	844.6	6.8	1873
PAO 100 +0.05 wt.% MWCNTs	809.8	5.2	1212

The EDS pattern of the worn surface of the ball tested in the presence of PPG 2000 containing 0.025 wt.% of MWCNTs (**Figures 4.16(b)-4.16(b_1)**) signify that the C peak, as well as it's atomic %, provides evidence for the formation of a thin tribo-film. Whereas EDS spectra of worn surface of disc lubricated by plain PPG 2000 (**Table 4.8**) show the higher atomic % of C, which was due to the presence of a large amount of wear debris on the surface (**Figures 4.14(a)-4.14(a_1)**). The wear particles are also composed of iron,

carbon, and oxygen. The PAO 100 with 0.05 wt.% MWCNTs-lubricated surface (**Figures 4.16(d)-4.16(d_1)**) has the lowest oxygen content and the highest carbon content among all tested surfaces, which imply that the polar functional group enables the adsorption of MWCNTs on the friction surface to form a lubricating film [139], which caused low wear (6.274×10^{-3} mm^3).

4.2.1.3. Proposed lubrication mechanisms

Based on the tribological results, analysis of the worn surfaces, and recent literature, a schematic lubrication mechanism for different lubricant formulations has been proposed and presented in **Figure 4.17**. For the surfaces lubricated with a plain base oil, only the oxide layer (tribo-layer) was formed between the friction pairs, which protected the surfaces up to a certain limit. However, with the progress of time and continuous tribological loading, this oxide layer breaks down, which leads to the removal of material at the interface due to metal-to-metal contact at the asperity. This phenomenon demonstrates an increase in friction and the combined action of various common wear mechanisms such as micro-ploughing and pits along with adhesion (as can be seen in **Figures 4.12** and **4.14)**) [140]. On the contrary, when COOH-functionalized MWCNTs were mixed in a plain base oil, the polar functional group facilitates the MWCNTs to be adsorbed on the friction surface to form a protective lubricating film, which separates the mating surface, thereby decreasing friction and wear. The high thermal conductivity of MWCNTs also enables resistance to friction heat, lowering the surface temperature and minimizing the probability of adhesion between the rubbing surfaces. It also ameliorates the lubricating effect owing to a unique hexagonal structure [141]. The MWCNTs easily enter into groves and openings of the rubbing surfaces, therefore, pressure can be disseminated over a large contact area, validating the mending effect. Furthermore, it is also presumed that the rolling effect of MWCNTs prevails throughout the entire friction

process because of the good ingrained stability of the additive between the mating surfaces. It may also be speculated that at a higher load, MWCNTs can be exfoliated into a lamellar shape (i.e., nanosheets of graphene), which deteriorated the rolling motion of MWCNTs, thereby increasing the COF (as evident in the case of PAO 100 with 0.05 wt.%) [65,135,136]. Nevertheless, these nanosheets stick to the surfaces and act as a solid lubricant, which contributes to the transfer layer formation at the interface of rubbing surfaces, thereby significantly diminishing the wear (**Figure 4.11**). The adhesion of these fragments may affect the surfaces of worn surfaces in terms of either degradation or comparable enhancement [139]. In this study, the worn surfaces lubricated with MWCNTs-based nanolubricants were relatively polished compared to the worn surfaces tested with plain base oils, as evident by SEM and SPM analyses.

Table 4.8: The summary of typical values of elements present on the worn surfaces of disc lubricated with different lubricant compositions

Lubricant composition	Weight %				Atomic %			
	Fe	C	Cr	O	Fe	C	Cr	O
Plain PPG 2000	61.46	29.06	1.06	8.43	27.06	59.49	0.50	12.95
PPG 2000+0.025 wt.% MWCNTs	76.46	21.19	1.54	1.63	42.21	54.40	0.91	2.65
Plain PAO 100	72.72	22.56	0.84	3.87	37.86	54.63	0.47	7.04
PAO 100 +0.05 wt.% MWCNTs	73.45	22.02	0.76	3.77	38.70	53.94	0.43	6.49

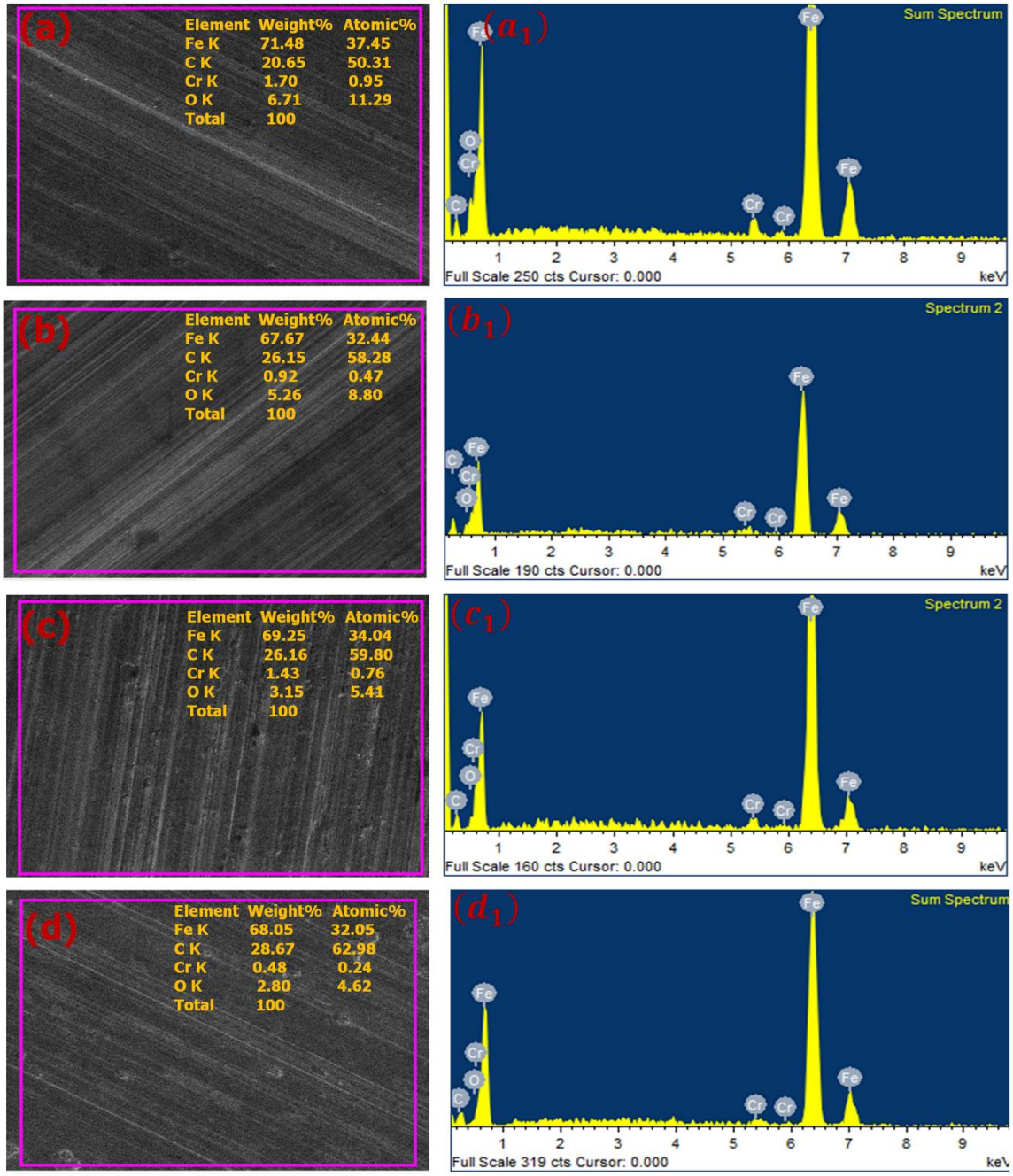

Figure 4.16: EDS spectra of wear scars of steel balls tested with (a, a_1) plain PPG 2000; (b, b_1) PPG 2000 with 0.025 wt.% MWCNTs; (c, c_1) plain PAO 100, and (d, d_1) PAO 100 with 0.05 wt.% MWCNTs. (Applied load: 300 N and test duration: 120 min)

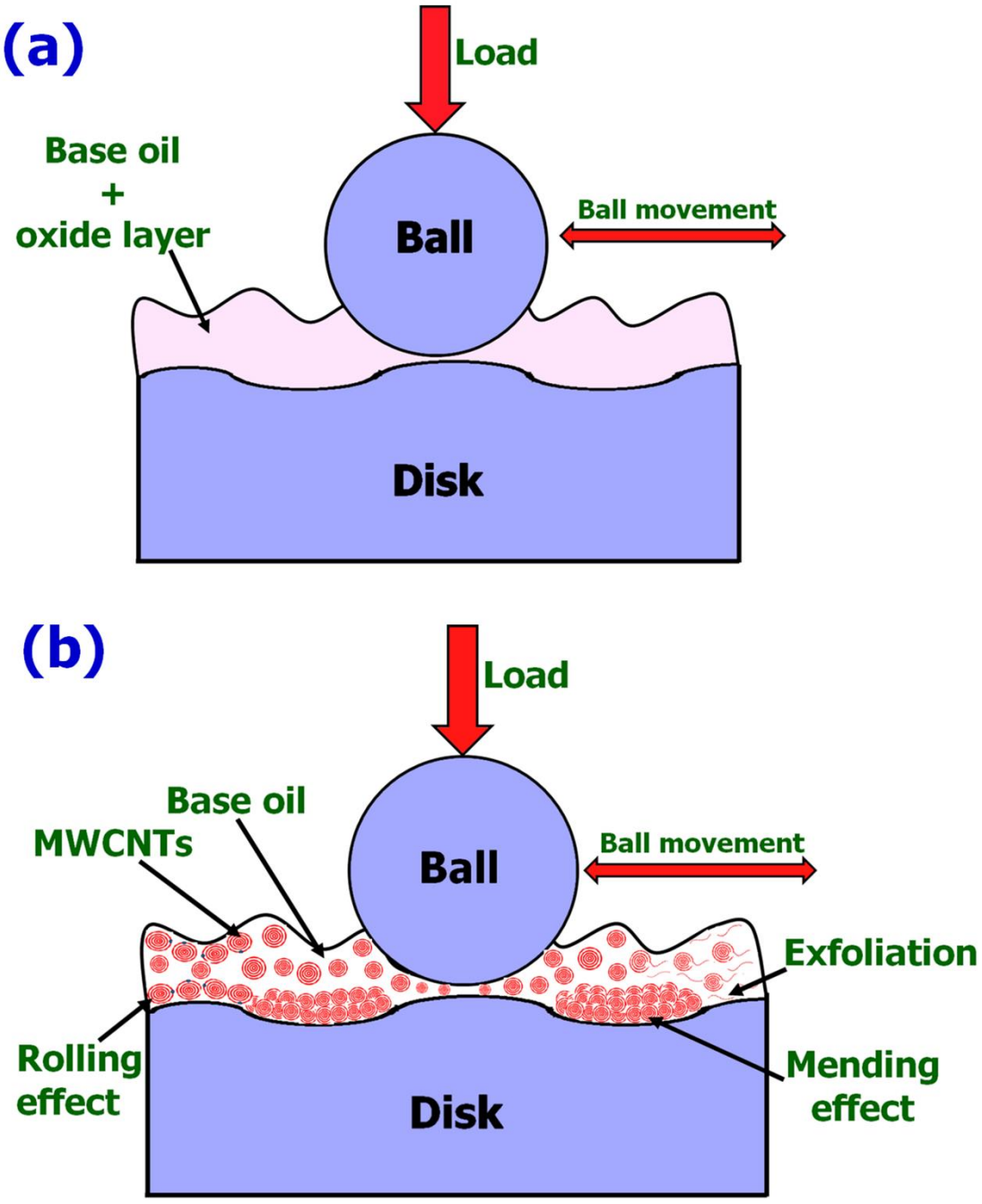

Figure 4.17: Lubrication mechanisms with (a) plain base oil, and (b) base oil containing MWCNTs

4.2.1.4. Investigation of MWCNTs stability in base Oils

The stability of additives in the base oils is an essential parameter for ensuring the performance of nanolubricants. The stability of nanolubricants was examined at room

temperature (~ 30 °C) by visual observation. The photographs of all nanolubricants at a varying concentration of MWCNTs were captured at different time periods, as shown in **Figure 4.18**. In both base oils, no evidence of sedimentation was observed at all concentrations of MWCNTs even after four months. **Figure 4.18(i)** displays the in-situ suspension mechanism and the role of the functional group. The hydrophilic segment of the functional group attached to the surface of MWCNTs and hydrophobic tail reacts with base oils. This phenomenon of modification of nanoadditive reduces the surface energy of MWCNTs, thereby enhancing the suspension stability of additives in the base oils for a more extended period.

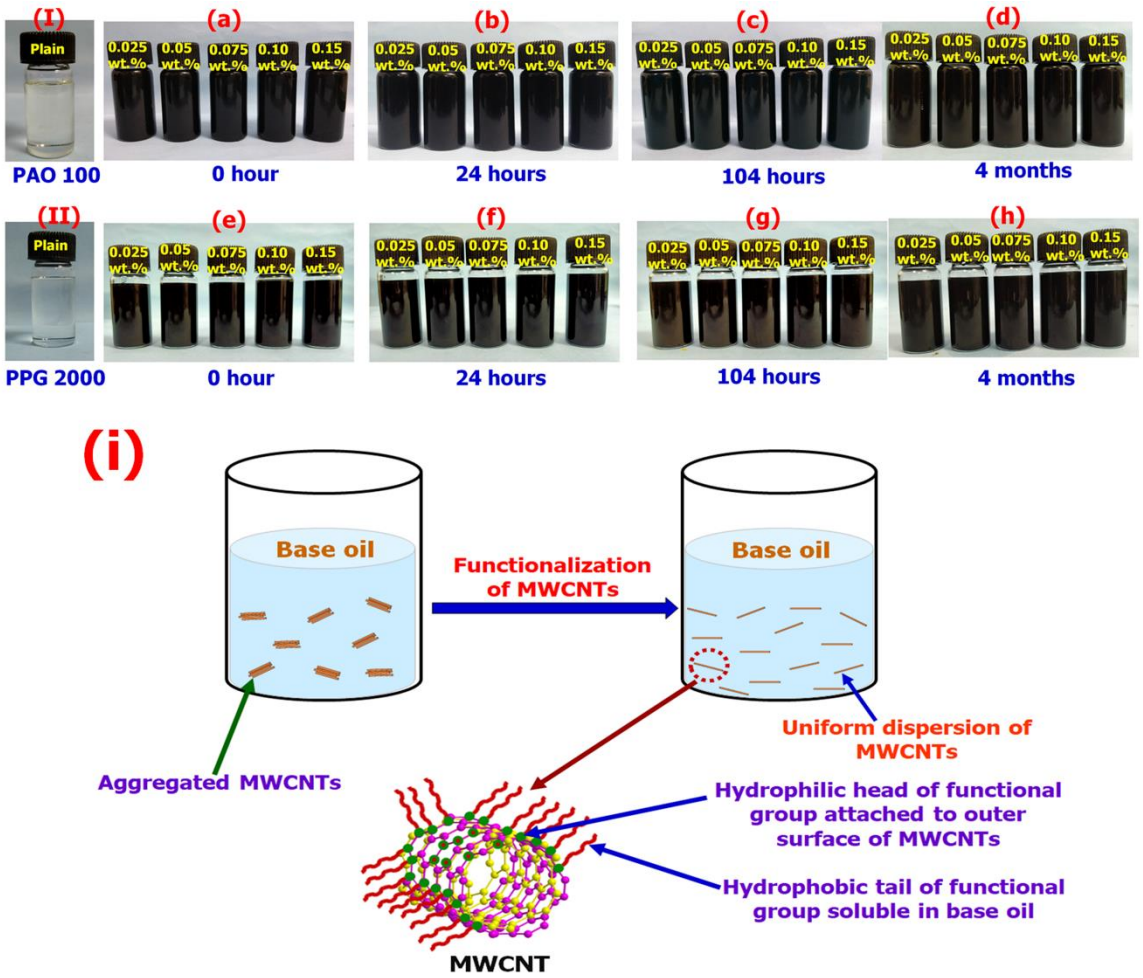

Figure 4.18: Photographs of MWCNTs suspension stability at different time intervals, (a-d) PAO 100 and (e-h) PPG 2000 at room temperature (~ 30 °C), and (i) demonstrates the role of the functional group in improving the dispersion stability in the base oils

4.2.2. Tribological evaluation of low viscosity synthetic base oils (PAO 4 and PAO 6) based nanolubricants

4.2.2.1. Friction and wear response of nanolubricants

Before the friction and wear test, extreme pressure (EP) tests were conducted according to ASTM D7421 standard to determine the load-carrying capacity of both base oils. The extreme pressure behaviour of both base oils is shown in **Figure 4.19**. According to the ASTM D7421 standard, the failure is indicated by a sharp rise in the COF more than 0.2 over the steady-state for over 20 s or a stoppage in the oscillating of the test machine. For PAO 4, the COF varies from 0.22 to 0.32 as load increases from 20 to 40 N for a test duration of 6 min, as displayed in **Figure 4.19(a)**. This implies that PAO 4 can sustain up to 40 N load without failure of lubricating film at the interface of friction pair. It is identified from **Figure 4.19(b)** that the COF in PAO 6 was continuously decreased till 34 min as load increased from 20 to 200 N, but there was a sudden rise in COF (~0.67) at 240 N after 34 min of test duration, followed by a decrement in COF till the end of the test. Therefore, 50 N was selected as a normal load in PAO 4 based nanolubricants. In contrast, for PAO 6 based nanolubricants, a normal load of 200 N was opted to conduct the friction and wear test. The details of test specifications are given in **Table 3.5**.

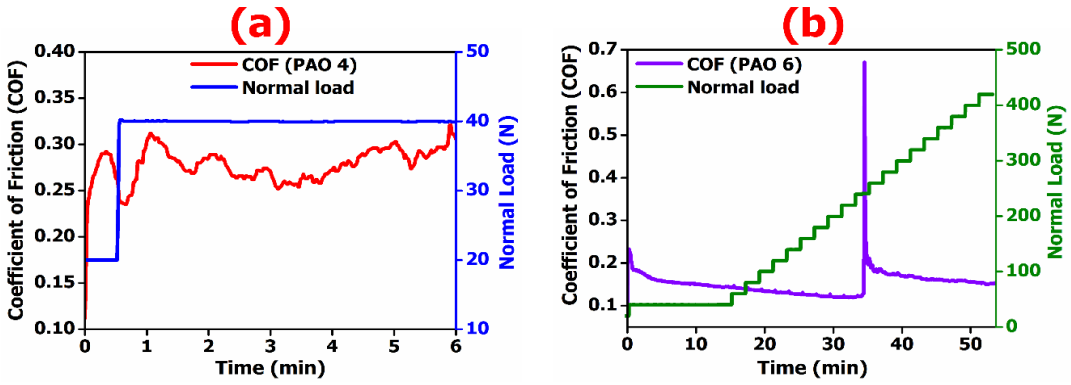

Figure 4.19: The EP behavior of (a) PAO 4 and (b) PAO 6 as per ASTM D7421

4.2.2.1.1. Antifriction responses of nanolubricants

The tribological properties of PAOs and PAOs with variable dose (0.025– 0.15 wt.%) of MWCNTs are shown in **Figure 4.20**. It is noticed from **Figure 4.20(a)** that MWCNTs have reduced the COF of both PAOs, but PAO 6 exhibited lower COF at all concentrations of additive as compared with PAO 4. In the previous studies, it is commonly reported that there is an optimal dose of nanoparticles in a base oil to obtain excellent tribological performance. For PAO 4, the minimum COF was observed at 0.05 wt.% dose of MWCNTs. However, it was also noticed that further increasing the dose of additive beyond 0.05 wt.% in PAO 4 results in a rise in COF, though it was less than plain PAO 4. The possible speculation for such behaviour of nanotubes may be that at an optimal dose, MWCNTs can efficiently be accumulated in the grooves and valleys of the tribo pairs and facilitate an effective rolling and mending effect. Consequently, COF has dramatically decreased. Moreover, another possible hypothesis is that generally, lubricants are squeezed out under a higher load. In the case of optimum dose, MWCNTs get adequate space and act as a useful spacer between the friction pairs. Due to tubular shape and superior mechanical properties, MWCNTs can roll between the rubbing surfaces in sliding friction, and consequently, the COF decreases. Whereas the existence of a higher dose of the additive can lead to the development of agglomeration of MWCNTs, which may mitigate the rolling effect, it may trigger ploughing action on the rubbing surfaces owing to hard and brittle attributes of MWCNTs and produces higher COF [129]. However, it can be ascertained with the frictional behaviour of PAO 6-based nanolubricants (**Figure 4.20(a)**) that the best anti-friction performance (minimum COF) was acquired at 0.075 wt.% of MWCNTs. The results mentioned above imply the positive frictional effect at a low dose of MWCNTs. The average COF for PAO 4 and PAO 6 at optimum concentration was 0.208 and 0.168,

respectively, and exhibited the maximum attenuation in COF approximately 27 and 8% compared with plain PAO 4 (0.286), PAO 6 (0.183), respectively.

Figure 4.20(b) shows the friction profiles of plain PAOs and PAOs with an optimal dose of MWCNTs. For plain PAO 4, the COF was very high at the initial stage of the experiment, followed by the fluctuation of COF for 10 min of test duration. After that, the COF continuously decreased with the test duration, and it fluctuated between 0.32 and 0.24, with an average COF of 0.286. The phenomenon of a remarkable increase in COF during the beginning of the test is called the running-in period. The hypothesis is that when new surfaces come in contact during the running-in period, a greater amount of wear is produced due to the rubbing of asperities until it establishes a stable phase, which increases the friction. The result illustrates that the oil film may not sufficiently to isolate the sliding contact, and a crucial metal-to-metal contact occurs during the running-in period. Nevertheless, the inclusion of 0.05 wt.% dose of MWCNTs into PAO 4 significantly decreased the running-in period time to ∼1 min, as well as the average COF was reduced considerably (i.e., 0.208). Moreover, the friction coefficient profile became smoother and achieved steady-state condition in 60 min of the test run. It is also observed from **Figure 4.20(b)** that the COF profile of plain PAO 6 was low compared to plain PAO 4 and PAO 4 comprising 0.05 wt.% of MWCNTs and exhibited less fluctuation throughout the test duration. Also, it was noticed that the addition of 0.075 wt.% concentration of MWCNTs into PAO 6, the frictional curve became more stable and followed a constant fluctuation in COF until the end of the experiment.

The power loss to overcome the friction (i.e., frictional power loss) during tribo testing was calculated using Eq. (4.1).

$$P_f = 2\mu n \Delta x W \tag{4.1}$$

Where, P_f represents the frictional power loss (MJ), μ is friction coefficient (COF), *n* is the number of cycles (362×10^3), Δx is the stroke length ($1 \times 10^{-3}\, m$), W is the applied normal load (50 N and 200 N for PAO 4 and PAO 6, respectively). The calculated power loss for both PAO-based nanolubricants is listed in **Table 4.9**. The frictional power loss is directly proportional to the applied load. Thus, PAO 6-based nanolubricants consumed more power to overcome frictional losses than PAO 4-based nanolubricants. Nevertheless, PAO 6-based nanolubricants exhibited a low COF at all concentrations of MWCNTs than PAO 4-based nanolubricant. However, with the inclusion of MWCNTs in both PAOs, power consumption was reduced significantly. The MWCNTs replenish frictional surface grooves and scars and make the friction surface sleek and uniform, decreasing the frictional force and lowering power consumption. PAO 4 containing 0.05 wt.% MWCNTs exhibited the maximum reduction (~26.3%) in power consumption. In PAO 6, the maximum reduction in power loss was obtained at 0.075 wt.% of additive (**Table 4.9**).

4.2.2.1.2. Anti-wear responses of nanolubricants

Figure 4.20(c) shows the change in WV with varying concentrations of MWCNTs for both PAOs. It can be observed that the inclusion of MWCNTs in both PAOs imparts a significant enhancement in anti-wear performance. Plain PAO 4 showed the greater WV (i.e., 52 × 10^{-3} mm^3), but the WV was reduced to a minimum level of about ~88% reduction with 0.025 wt.% of additive in PAO 4. Further increasing the amount of MWCNTs in PAO 4 from 0.05 to 0.15 wt.%, the wear volume rises continuously. Therefore, the lowest wear (~ 6×10^{-3} mm^3) was obtained at 0.025 wt.% of MWCNTs. Although at a dose of 0.075 wt.% of additive in PAO 4, there was an abrupt acceleration in wear, and it was inferior compared with plain PAO 4. The possible hypothesis behind this phenomenon might be a mechanism of development and deterioration of fluid film caused by the aggregation of MWCNTs followed by the three-body abrasion. This will increase the wear of the sliding pairs and

the COF. This may be the possible known wear mechanisms. It was also noticed that plain PAO 6 exhibited lower WV than plain PAO 4. In contrast, MWCNTs were unable to significantly impact the anti-wear performance of PAO 6, as witnessed in the case of PAO4 containing MWCNTs. The probabilistic rationale for this behaviour may be that PAO 6 based nanolubricants were tested at 200 N corresponding Hertzian stress of 2.74 GPa, which is very high, whereas PAO 4 nanolubricants which were tested at 50 N load corresponding Hertzian stress of 1.73 GPa. In PAO 6, the minimal wear volume (i.e., ~ 26.8×10^{-3} mm^3) was attained at 0.05 wt.% dose of MWCNTs and offered a maximum reduction in wear volume (~ 27%).

4.2.2.2. Worn surfaces analysis

4.2.2.2.1. Worn surface analysis of steel balls

Figure 4.21 displays the SEM micrographs of steel balls tested with plain PAOs and PAOs containing MWCNTs. A more prominent wear scar with peeling pits and micro-abrasive, as well as deep scratches, appeared along the sliding direction when tested with plain PAO 4 (**Figures 4.21(a)** and **4.21(b)**). This might be due to the loss of tribo-film on the worn surface, which leads to surface-originated spalling. However, comparably smallest wear scar and smooth surface with only a few shallow and slender grooves were identified when tested with PAO 4 incorporating 0.025 wt.% MWCNTs as shown in **Figures 4.21(c)-4.21(d)**. The results imply that much of the wear occurred by removing top asperities through the polishing mechanism. These findings affirm the wear and friction results, as displayed in **Figure 4.20**.

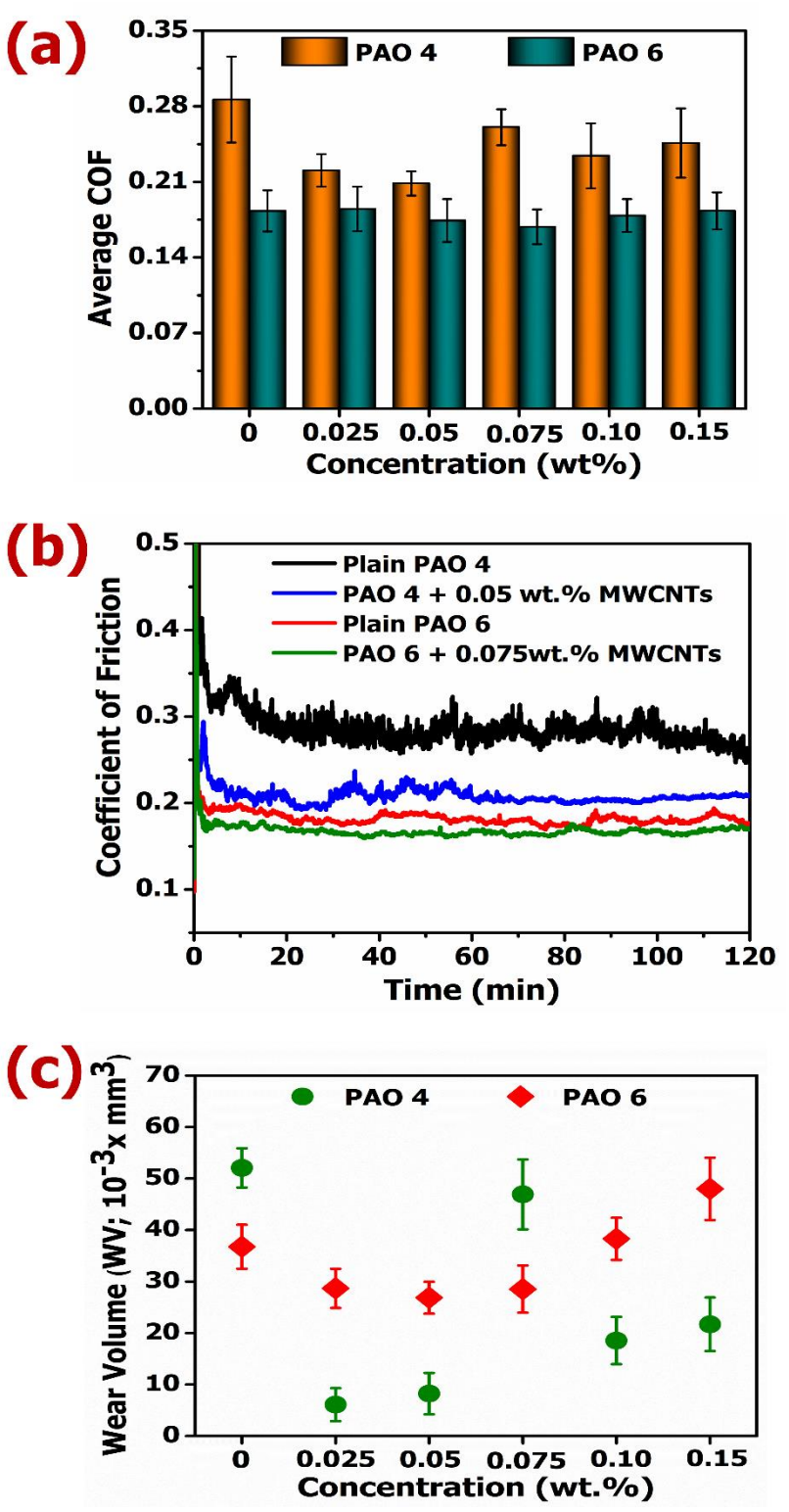

Figure 4.20: (a) The average COF with variable concentration of MWCNTs in PAOs, change in (b) COF as a function of test duration, and (c) WV with varying doses of additive. (Applied load: 50 N for PAO 4 and 200 N for PAO 6-based nanolubricants and test duration: 120 min)

Table 4.9: Summary of frictional power loss at different concentrations of additives

Base oils	Parameter	MWCNTs concentration (wt.%)					
		0	0.025	0.05	0.075	0.1	0.15
PAO 4	Frictional power (MJ)	10.1	8.3	7.4	9.4	7.8	8.3
	Percentage reduction	-	17.3	26.3	6.6	22.6	17.7
PAO 6	Frictional power (MJ)	25.9	27.0	25.0	24.1	26.7	26.3
	Percentage reduction	-	-4.1	3.4	6.8	-3.1	-1.5

The worn surface lubricated by plain PAO 6 (**Figures 4.21(e)** and **4.21(f)**) demonstrated the smaller wear scar as well smoother surfaces compared with worn surfaces tested with plain PAO 4 (**Figures 4.21(a)** and **4.21(b)**). The reason is that PAO 6 featured better viscous characteristics (i.e., higher VI and higher viscosity) in comparison to PAO 4 leads to the development of relatively thick film at the interfaces of mating surfaces. Furthermore, plain PAO 6 showed a higher value of thickness ratio (λ) than plain PAO 4. It is noticed from **Figures 4.21(g)** and **4.21(h)** that incorporating MWCNTs in PAO 6 lowered the wear scar dimension and the intensity of abrasive grooves. The results showed that lubrication performance was substantially enhanced after the introduction of MWCNTs in both PAOs.

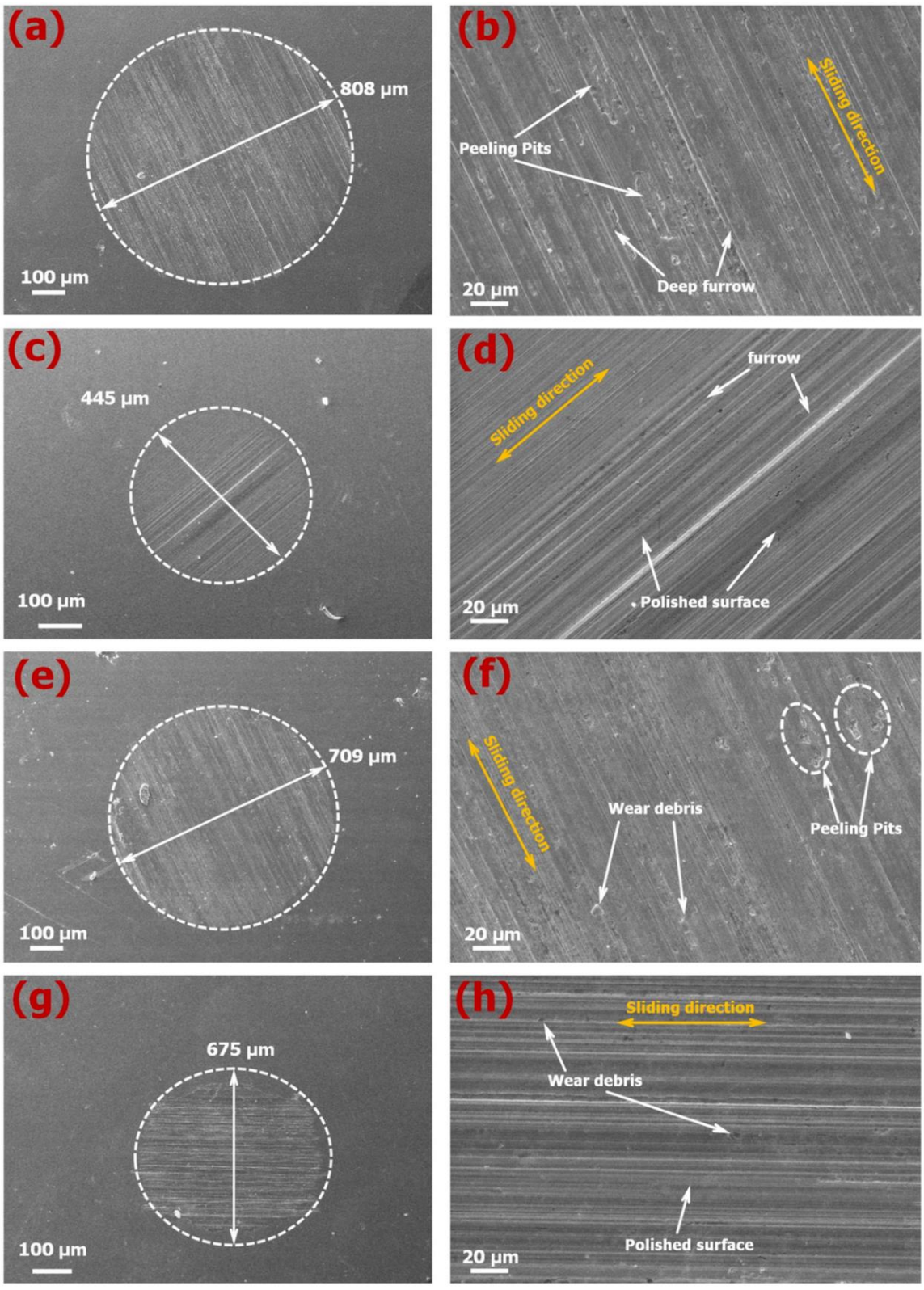

Figure 4.21: Worn surfaces of steel balls tested with (a, b) Plain PAO 4; (c, d) PAO 4 containing 0.025 wt.% MWCNTs; (e, f) Plain PAO 6, and (g, h) PAO 6 containing 0.05 wt.% MWCNTs. [Note: - a, c, e, g: at 200X; and b, d, f, h: at 1000X] (Applied load: 50 N for PAO 4 and 200 N for PAO 6-based nanolubricants and test duration: 120 min)

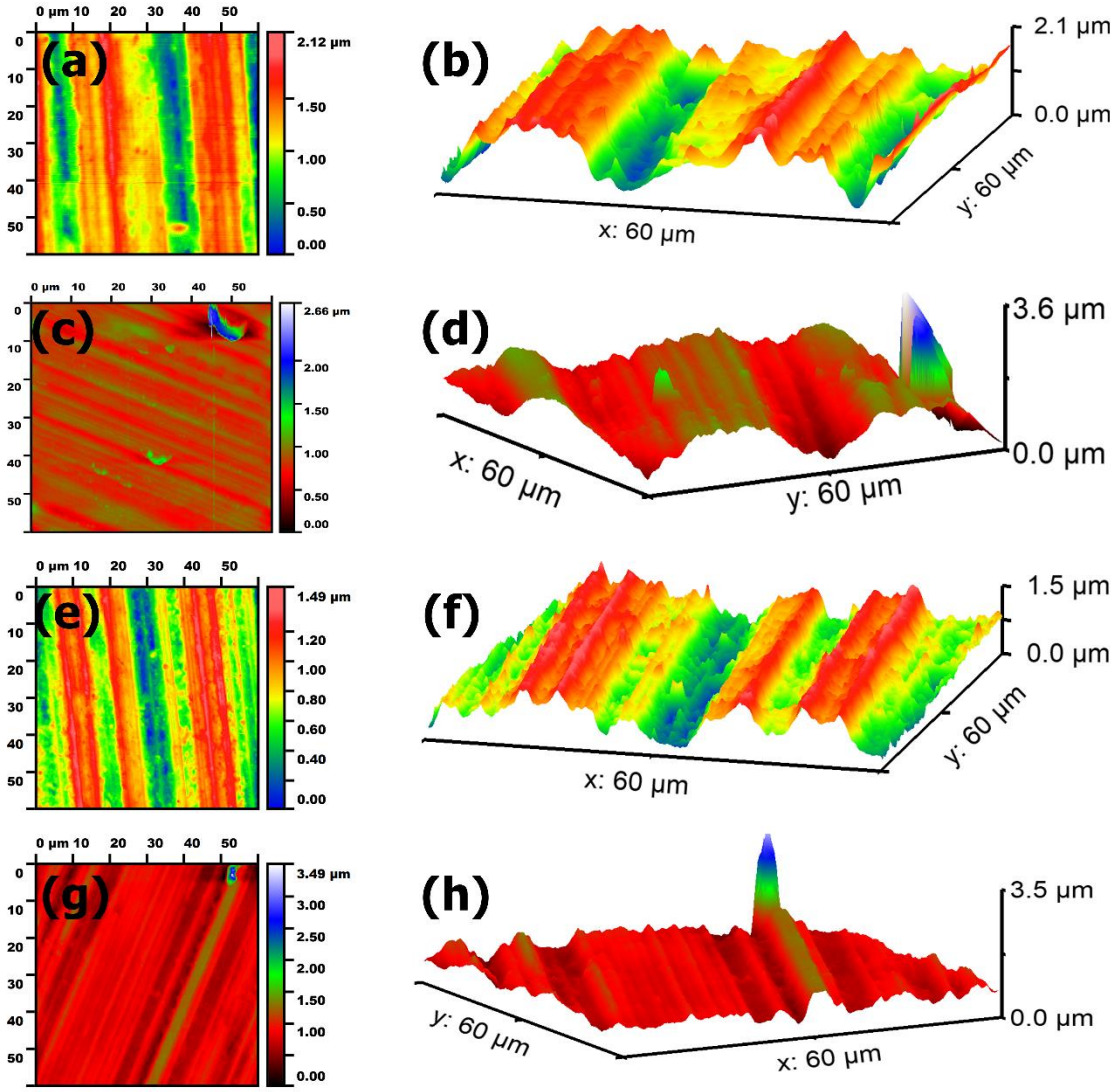

Figure 4.22: Topographic micrographs of steel balls lubricated by (a, b) plain PAO 4; (c, d) PAO 4 containing 0.025 wt.% MWCNTs; (e, f) Plain PAO 6, and (g, h) PAO 6 containing 0.05 wt.% MWCNTs. [Note: - a, c, e, g: Top view and b, d, f, h: Three-dimensional view of worn surfaces] (Applied load: 50 N for PAO 4 and 200 N for PAO 6-based nanolubricants and test duration: 120 min)

The topography of worn steel balls was also probed by using SPM. The topographic micrographs of two-dimensional (2D) and three-dimensional (3D) view and corresponding roughness values of worn surfaces of steel balls tested with plain PAOs and PAOs containing MWCNTs are arranged in **Figure 4.22** and **Table 4.10**, respectively. Figure 4.22(a) shows the deflection image (top view) of the worn surface lubricated with plain PAO 4, signifying that the worn surface was rough in appearance and furrows were more profound. The surface roughness (Sq) was determined to be 389.4 nm. Besides, the 3D

micrographs (**Figure 4.22(b)**) featured the occurrences of severe abrasive and adhesive wear on the worn surface, which led to higher COF and wear (**Figure 4.20**). Meanwhile, the addition of 0.025 wt.% in PAO 4 (**Figures. 4.22(c)** and **4.22(d)**) demonstrated shallower groves along with a relatively polished surface, which designated the effective mitigation of severe abrasive wear. Consequently, the surface roughness was reduced to 142.5 nm. The surface roughness (Sq) of worn surface lubricated with plain PAO 6 and PAO 6 containing 0.05 wt.% MWCNTs were ascertained to be 288.3 and 198.1 nm, respectively, and exhibited a reduction of ~32%. A sharp asperity was observed in the topographic micrographs (3D view) of both PAOs containing MWCNTs. The peeling pit, apparent in the right corner of the deflection image, is the source of increasing the height of asperity. Apart from this single asperity, the worn surface appears to be more uniform.

The topography of the worn surfaces of steel ball lubricated with plain PAOs and PAOs containing MWCNTs was further investigated using the bearing area ratio (BAR) curve to analyse the influence of various statistical parameters on friction and wear. The BAR curve is defined as a plot drawn between the percent bearing area ratio as abscissa and asperity heights (depth) as ordinate, obtained from the 2D roughness profile of worn surfaces [142]. The BAR curve along with the linear roughness profile of the worn surface of steel balls are arranged in **Figure 4.23**, and **Table 4.10** represents the values of various roughness parameters which were extracted from the BAR curve (i.e., S_k, S_{pk}, S_{vk}, S_{r1}, S_{r2}) and from 2D roughness profile (i.e., S_a, S_q, S_{sk}, S_{ku}). The BAR curve can be segmented into three zones: The upper zone is expressed as reduced peak height (S_{pk}), the middle as core zone (S_k), and the lower zone as reduced valley depth (S_{vk}). The parameters S_{r1} and S_{r2} were also extracted from the BAR curve, representing the percentage of bearing area ratio found in the limits of the core profile. The illustration of all notations is shown in **Figure 4.23(a)**. The peak region is generally worn out when two surfaces rub together; the core zone

sustains the load and affects the longevity of the components, and the valley zone functions as a lubricant reservoir [143]. It is noticed from **Figures 4.23(a)** and **4.23(c)** and **Table 4.10** that the S_k, S_{pk}, S_{vk}, S_{r1} values of worn surface lubricated by PAO 4 containing MWCNTs were reduced, and the value of S_{r2} was increased as compared with plain PAO 4. This implied that peaks on the worn surface were polished off, and valleys were filled by MWCNTs, which led to flattening the middle region of its BAR curve. Consequently, a comparably polished or smooth surface was obtained, as shown in SEM and SPM micrographs (**Figures 4.21** and **4.22**). For worn surface related to plain PAO 4, the value of S_{vk} was greater than the value of S_{pk}, which inferred that PAO 4 was stored in the valley region and served as a lubricant. However, it was also presumed that the lubricants are generally squeezed out under higher loading conditions, leading to asperity-to-asperity contact. Therefore, higher friction and wear was observed, as displayed in **Figure 4.20**. Although, in the case of PAO 4 comprising MWCNTs, S_{vk} became smaller than the value of S_{pk}. The diminutive dimensions of MWCNTs enable them to infiltrate and deposit into the space of valleys and validating the mending effect. Also, MWCNTs serve as an efficient intercessor (i.e., solid lubricant due to unique hexagonal structure), confining between the tribo pairs [129]. Liu et al. [144] identified the mending effect as a mechanism for copper nanoparticles on a tribological surface, and its deposition on the worn surface has reduced the loss of wear. The same behaviour was observed when MWCNTs were added into PAO 6, as shown in **Figure 4.23(g**). Among all BAR curves (**Figure 4.23**), worn surface lubricated by PAO 4 incorporating 0.025 wt.% doses of MWCNTs demonstrated the flattest curve. The roughness parameters (R_a , R_q, S_{sk}, S_{ku}) were also probed to correlate their impact on the tribological performances for different lubricant compositions and are listed in **Table 4.10**. The centre line average (i.e., R_a) is an important roughness parameter, but two different surfaces may have similar R_a value and may function differently. Therefore,

it is necessary to analyse other parameters such as S_{sk}, and S_{ku}. The S_{sk} is defined as the skewness, and it is sensitive to occasional deep valleys or high peaks. On the other hand, kurtosis (S_{ku}) describes the probability density sharpness of the profile. It is noticed from **Table 4.10** that worn surfaces lubricated with PAOs containing MWCNTs demonstrated a positive value of S_{sk} as well as S_{ku} (>3). The results illustrated that doping of MWCNTs in PAOs alleviated the valleys of surfaces, also increased the height of asperity (only at one location as displayed in **Figure 4.22**), which resulted in an enhancement in the tribological performance of PAOs. The negative S_{sk}, and S_{ku}values of worn surfaces lubricated by plain PAOs supported the theory that mildly worn asperities resulted in the surface being more negatively skewed by exhibiting more pits and valleys than peaks [143] as manifested by SPM micrographs (**Figure 4.22**).

4.2.2.2.2. Worn surface analysis of counterpart (disc)

The SEM images of worn discs tested with plain PAOs and PAOs with MWCNTs are displayed in **Figure 4.24**. The cross-sectional profiles of the wear track on the disc are shown in Figure 4.25. These profiles were employed to assess various surface parameters, such as wear track depth and cross-sectional wear area (W_q). As shown **in Figures 4.24(a) and 4.24(b)**, the worn surface of the disc specimen tested with plain PAO 4 showed greater wear track width of 802 µm with a deep furrow in which abrasive ploughing was the prominent wear mechanism. Moreover, a lot of spalling pits were observed on the wear track along the sliding direction. The same features are also observed in **Figures 4.21(a) and 4.21(b)**, which might be the rationale for the highest friction and wear (**Figure 4.20**). Moreover, the profile curve is shown in **Figure 4.25(a)** exhibited the deepest and broadest wear scar, which has a maximum wear depth of 4.87 µm and a cross-sectional wear area of 1015 μm^2. In contrast, no signs of spalling pits were identified. Comparably polished surfaces with shallow furrows evidenced the considerable reduction in abrasive ploughing

intensity when friction pairs were lubricated by PAO 4 containing 0.025 wt.% dose MWCNTs as shown in **Figures 4.24(c)** and **4.24(d)**.

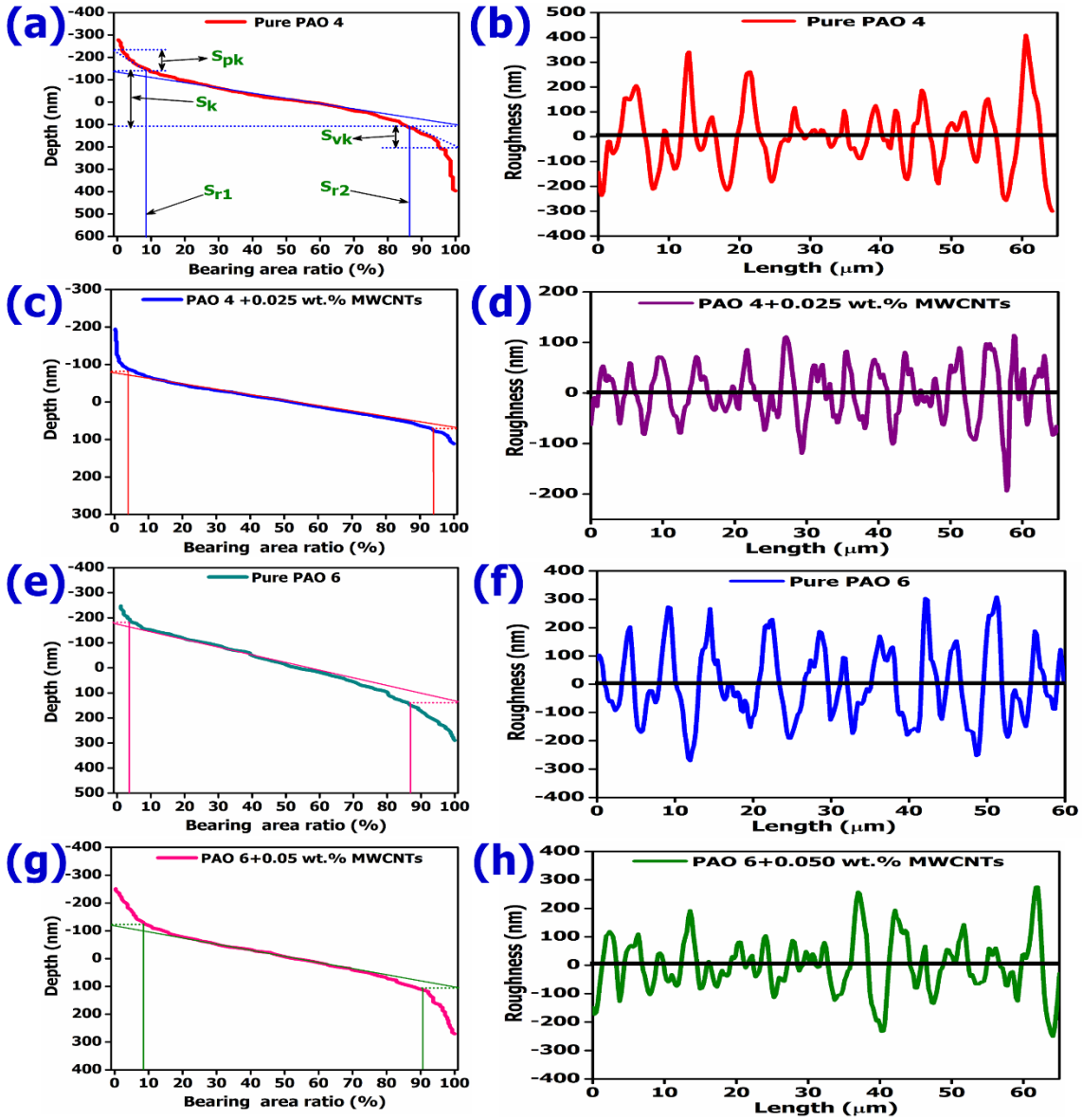

Figure 4.23: Bearing area ratio curve and respective linear roughness profiles of steel balls tested with (a, b) Plain PAO 4; (c, d) PAO 4 containing 0.025 wt.% MWCNTs; (e, f) plain PAO 6 and (g, h) PAO 6 containing 0.05 wt.% MWCNTs. (Applied load: 50 N for PAO 4 and 200 N for PAO 6-based nanolubricants and test duration: 120 min)

Table 4.10: Surface roughness parameter of worn steel balls tested various lubricant formulations

Lubricant composition	Line roughness		Surface roughness		Morphological Parameter						
	R_a (nm)	R_q (nm)	S_a (nm)	S_q (nm)	S_{sk}	S_{ku}	S_k (nm)	S_{pk} (nm)	S_{vk} (nm)	S_{r1} (%)	S_{r2} (%)
Plain PAO 4	97.2	127.5	317	389.4	-0.48	-0.52	243.2	115.5	132.4	8.5	86.5
PAO 4+0.025 wt.% MWCNTs	41.4	50.6	80.8	142.5	3.1	29.9	154.5	46.6	28.5	4.1	93.8
Plain PAO 6	106.4	128.1	240.8	288.3	-0.13	-0.74	318.4	88.9	119.1	3.4	86.9
PAO 6+0.05 wt.% MWCNTs	74.6	96.1	143.3	198.1	1.7	14.2	227.1	80.9	107.7	8.3	90.6

MWCNTs tend to form thin lubricant film, covering the surface asperities and promoting smooth surfaces. The MWCNTs in contact with mating surfaces may slip and slide and impart shielding against high frictional forces. This explains the combined presence of abrasive grooves and polished smooth surfaces on the wear scars produced by PAO 4 with MWCNTs [145]. Consequently, a minimum wear scar on the steel disc with a minimum wear track width of 442 µm was obtained, and the corresponding wear depth and wear area were decreased to 3.64 µm and 229 μm^2, respectively. For the surfaces lubricated with plain PAO 6, the wear track width, average depth, and cross-sectional wear area were estimated to be 754 µm, 4.69 µm, and 989 μm^2, respectively, as displayed in **Figures 4.24(e)** and **4.25(c)**. Whereas the inclusion of 0.05 wt.% MWCNTs into PAO 6, the wear track width, depth, and cross-sectional area of the worn surface were significantly abated to 692 µm, 4.43 µm, and 432 μm^2, respectively, which is also affirmed by SEM results of the worn surface of the disc (**Figures 4.24(g)-4.24(h)**).

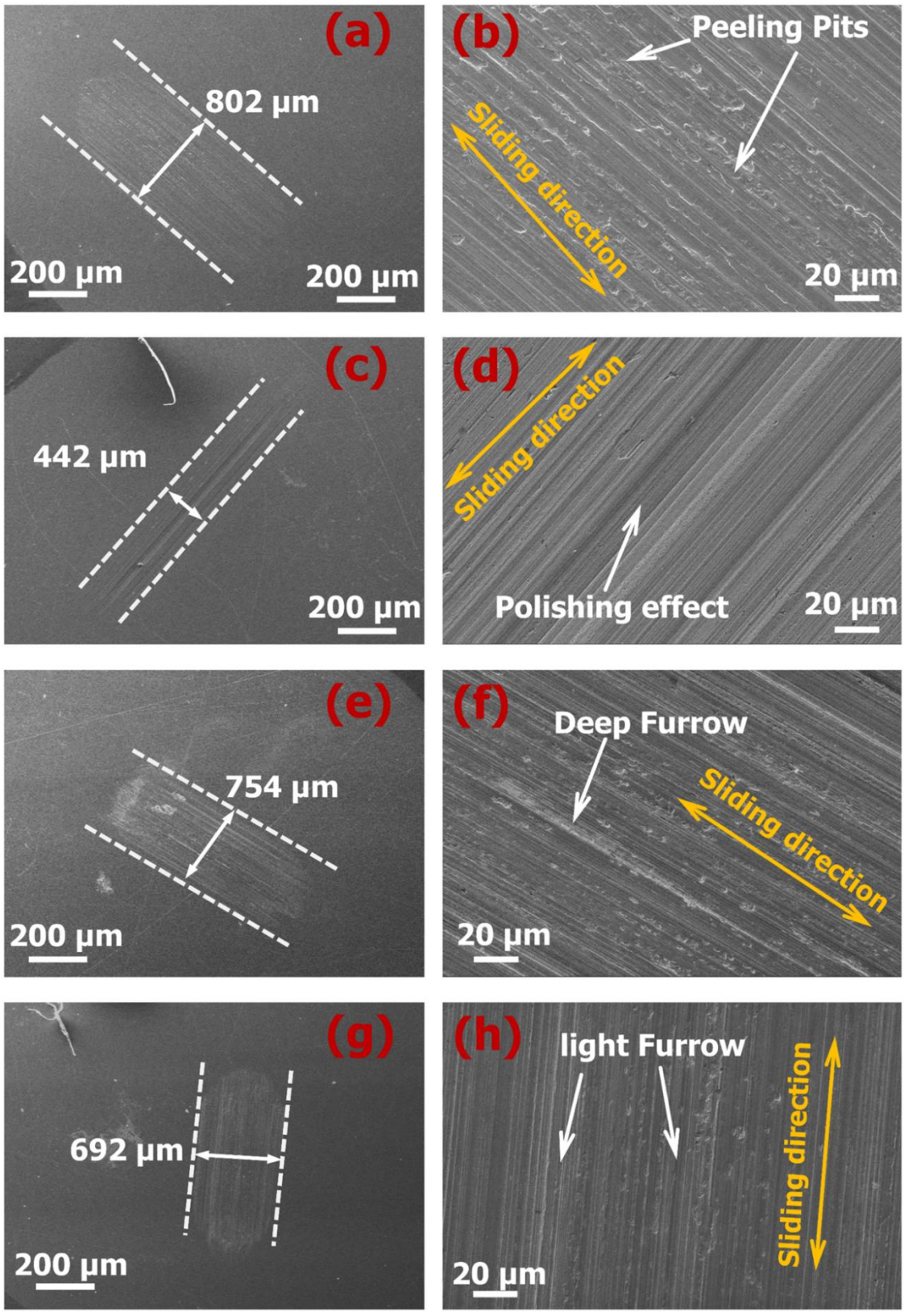

Figure 4.24: SEM images of worn surfaces of disc in friction test lubricated with (a, b) Plain PAO 4; (c, d) PAO 4 containing 0.025 wt.% MWCNTs; (e, f) Plain PAO 6, and (g, h) PAO 6 containing 0.05 wt.% MWCNTs. [Note: - a, c, e, g: at 60X; and b, d, f, h: at 500X] (Applied load: 50 N for PAO 4 and 200 N for PAO 6-based nanolubricants and test duration: 120 min)

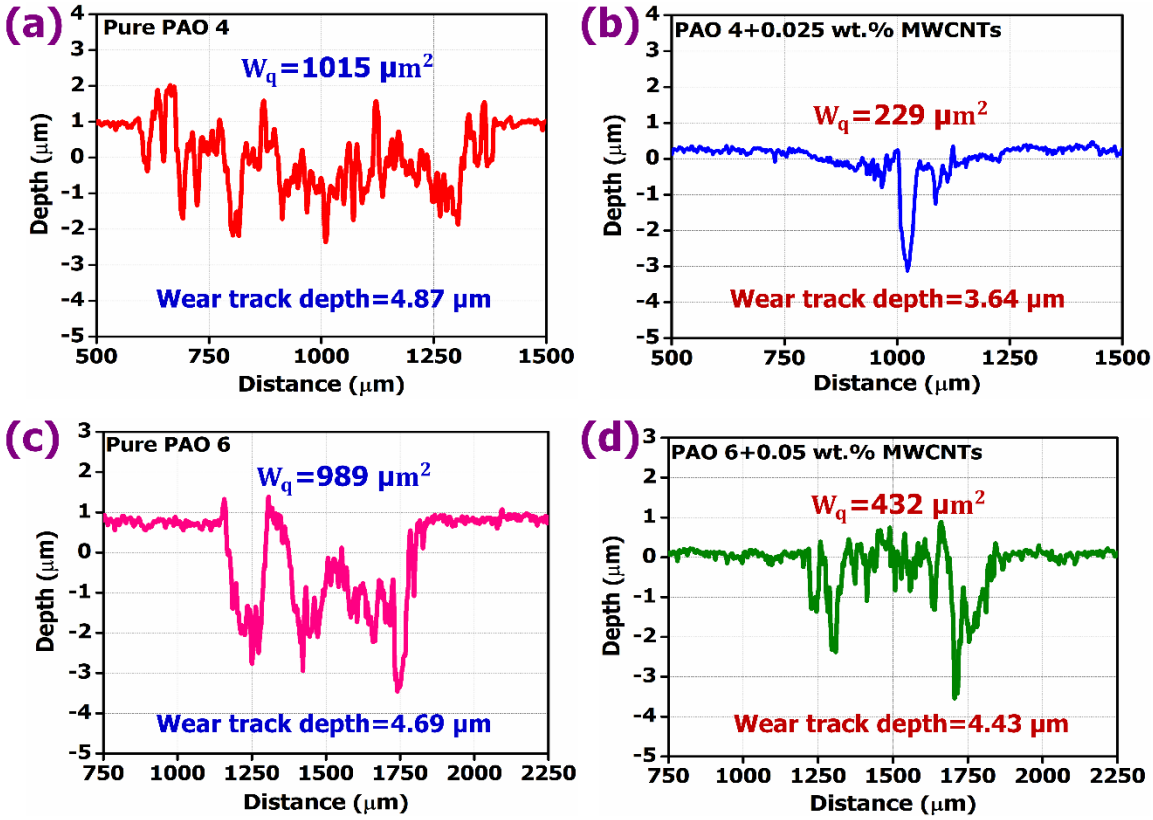

Figure 4.25: The surface profile of wear track of the disc tested with (a) Plain PAO 4; (b) PAO 4 comprising 0.025 wt.% MWCNTs; (c) Plain PAO 6, and (d) PAO 6 containing 0.05 wt.% MWCNTs. (Applied load: 50 N for PAO 4 and 200 N for PAO 6-based nanolubricants and test duration: 120 min)

4.2.2.2.3. EDS analysis of worn surfaces

Figure 4.26 and **Table 4.11** illustrate the EDS spectrum and weight% and atomic% of individual elements of the selected rubbed surfaces of steel balls and discs, respectively. The film formation phenomenon is complicated and depends on how easily nanoparticles enter into grooves of friction pairs and get smeared, leading to the film formation. It is noticed from **Figure 4.26** and **Table 4.11** that the EDS spectrum exhibited the existence of iron, carbon, chromium, and oxygen on all the worn surfaces. EDS array of the worn surface of ball tested with plain PAO 4 (**Figures 4.26(a)-4.26(b)**) exhibits the higher carbon%, which may be attributed to metal transfer due to surface-originated spalling or plastic deformation from the mating disc (**Table 4.11**). The traces of carbon found on the worn surfaces lubricated by plain PAOs may be due to the hydrocarbon degradation of

olefins or due to steel ball and disc. Furthermore, the substantial presence of oxygen means that oxide layers were formed during friction tests when iron reacted with air. It is noticed from **Figure 4.26** and **Table 4.11** that higher atomic% of carbon and lower atomic% of oxygen have appeared at worn surfaces tested with PAOs containing MWCNTs compared with plain PAOs. This is strong evidence that MWCNTs were adsorbed on the rubbing surface to form a tribo-film. Consequently, a smooth surface was obtained, as discussed previously in the SEM analysis section of the ball and disc (**Figures 4.21** and **4.24).** This developed lubricating oil film (tribo-film) plays a prominent role in describing the enhanced tribological characteristics of both PAOs (as shown in **Figure 4.20**)

Table 4.11: The elements present on the worn surfaces of disc lubricated with various lubricants

Lubricant composition	Weight %				Atomic %			
	Fe	C	Cr	O	Fe	C	Cr	O
Plain PAO 4	79.44	14.54	1.14	4.88	48.05	40.91	0.74	10.29
PAO 4+0.025 wt.% MWCNTs	78.29	18.95	0.95	1.82	45.05	50.71	0.59	3.65
Plain PAO 6	78.01	18.41	0.73	2.85	46.08	52.54	0.70	10.69
PAO 6 +0.05 wt.% MWCNTs	73.66	23.84	0.54	1.96	37.47	57.10	0.31	5.12

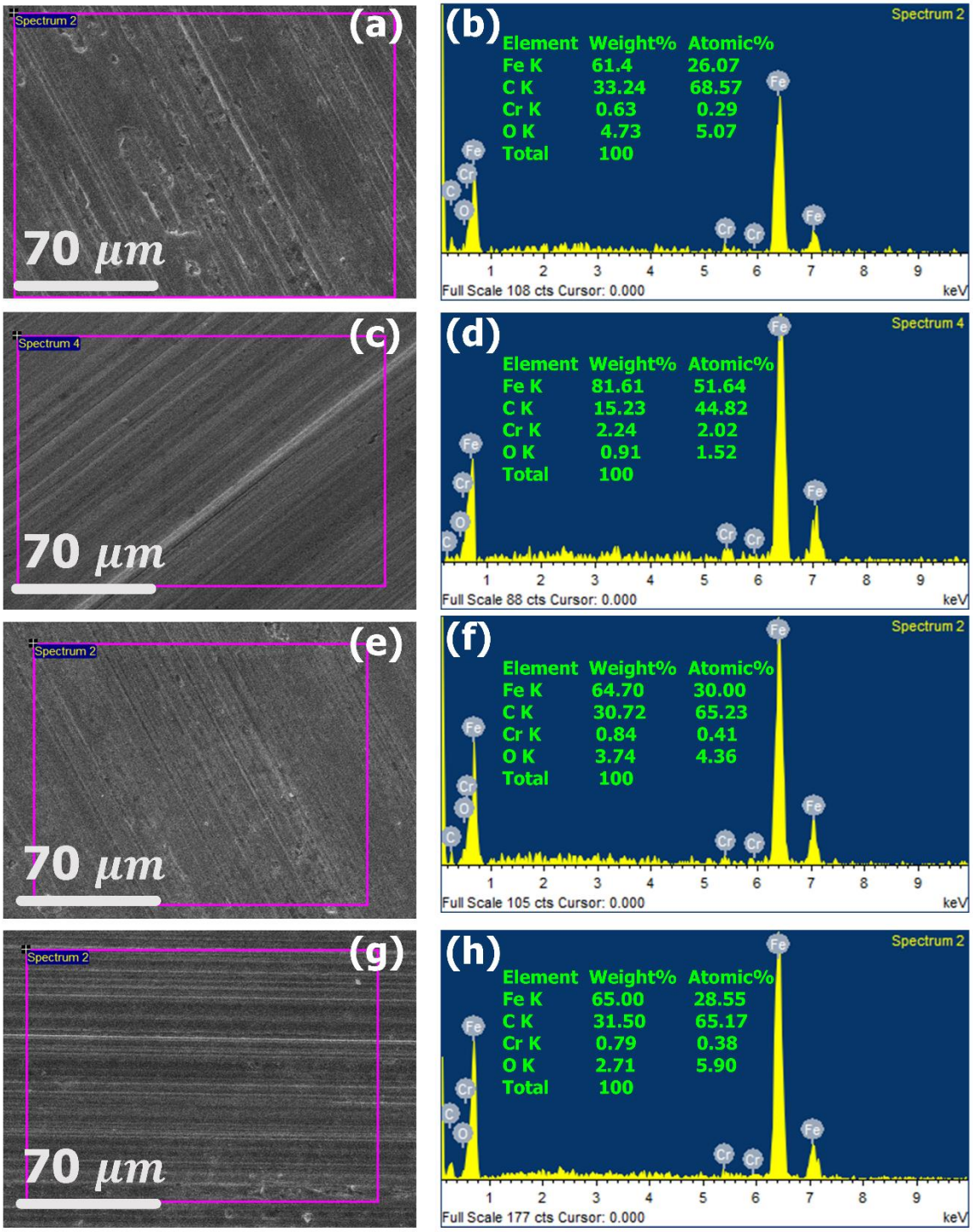

Figure 4.26: EDS spectrum of worn scars of steel balls lubricated by (a, b) Plain PAO 4; (c, d) PAO 4 containing 0.025 wt.% MWCNTs; (e, f) Plain PAO 6, and (g, h) PAO 6 comprising 0.05 wt.% MWCNTs. (Applied load: 50 N for PAO 4 and 200 N for PAO 6-based nanolubricants and test duration: 120 min)

4.2.2.2.4. XPS analysis of worn surfaces

The worn surfaces of ball and disc were further probed by XPS to identify the chemical states of the individual elements of the tribo-film formed in situ and shown in **Figures 4.27** and **4.28**. The Fe 2p, O 1s, and C 1s peaks were detected on all worn surfaces as displayed in Figures **4.27(a)** and **4.27(b)**, suggesting that PAO base oil molecules or MWCNTs were adsorbed on the interface and reacted with the iron-based worn surface. It was also observed that the oxygen component on the worn surfaces of the disc and ball (**Figure 4.27**) decreased significantly with the addition of MWCNTs. This was the reason for reduced friction, frictional heat, and oxidation of steel ball and disc surfaces. These results are correlated well with the EDS analysis (**Figure 4.26** and **Table 4.11**). The carbon component has appeared on all worn surfaces of the ball and disc because carbon is the main element of both test specimens.

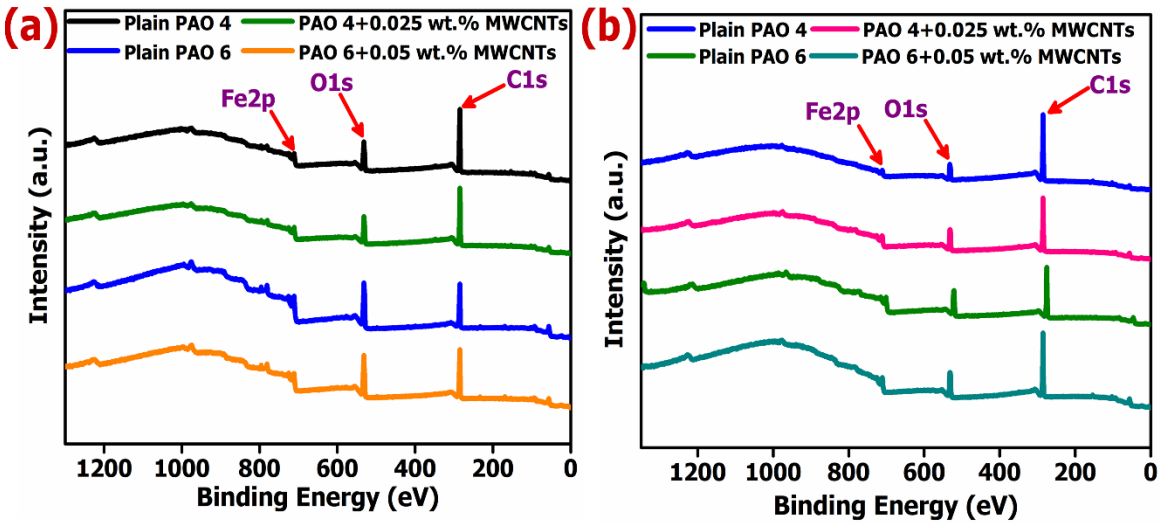

Figure 4.27: XPS spectra of worn surface of (a) disc, and (b) ball lubricated by various lubricant compositions. (Applied load: 50 N for PAO 4 and 200 N for PAO 6-based nanolubricants and test duration: 120 min)

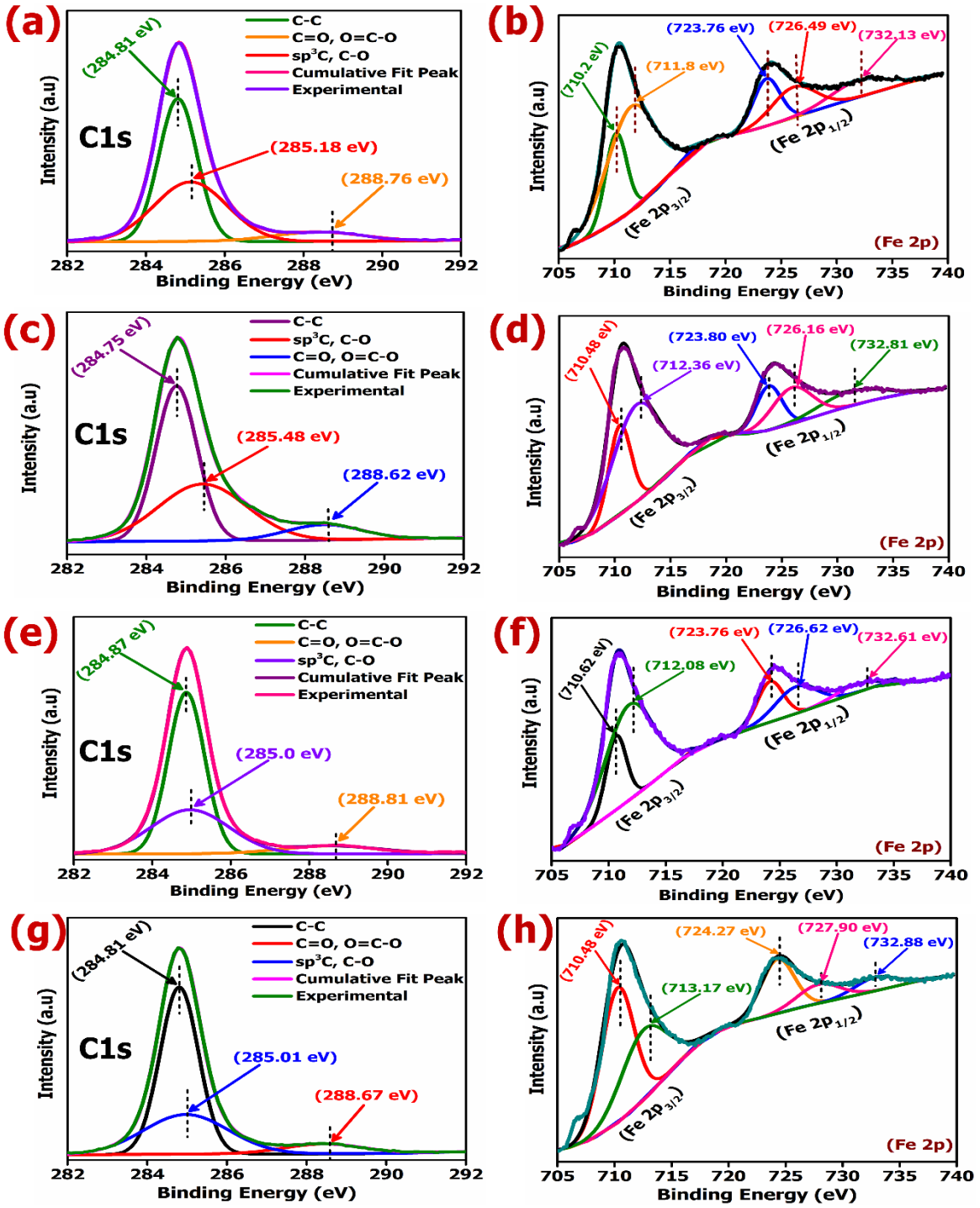

Figure 4.28: Deconvoluted XPS spectra of worn surface of disc lubricated by (a, b) PAO 4 containing 0.025 wt.% MWCNTs; (c, d) PAO 6 comprising 0.05 wt.% MWCNTs, and deconvoluted XPS spectra of wear scar of ball lubricated by (e, f) PAO 4 containing 0.025 wt.% MWCNTs; (g, h) PAO 6 with 0.05 wt.% MWCNTs. (Applied load: 50 N for PAO 4 and 200 N for PAO 6-based nanolubricants and test duration: 120 min)

The deconvoluted XPS spectra of C 1s and Fe 2p of worn surfaces of tested disc and ball are displayed in **Figure 4.28**. The three peaks in C 1s spectra of tested disc lubricated by PAO 4 with 0.025 wt.% MWCNTs were appeared at 284.81 eV, 285.18 eV, and 288.76

eV, respectively (**Figure 4.28(a)**), which are assigned to C–C, C–O/sp^3C, and C=O/O=C–O, respectively [146,147]. Since sp^3 C bonding is the key property of MWCNTs in achieving excellent toughness, wear resistance protects the rubbing pairs effectively. The spectra of Fe 2p can be deconvoluted into five peaks located at 710.2 eV, 711.8 eV, 723.76 eV, 726.49 eV, and 732.13 eV, as shown in **Figure 4.28(b)**. The Fe 2p peaks at 710.2 eV and 723.76 eV together confirmed the presence of Fe_2O_3. The peak that appeared at 711.8 eV is credited to FeOOH. The Fe 2p located at 710.2 eV and 723.76 eV are assigned to the Fe 2p3/2 and Fe 2p1/2. However, two peaks located at 726.49 and 732.13 eV, suggest complex iron oxides [148]. The results from XPS analysis of worn surfaces of disc lubricated by PAO 6 containing 0.05 wt.% MWCNT (**Figures 4.28(c)** and **4.28(d)**) and worn surface of ball lubricated by PAOs containing an optimum concentration of MWCNTs (**Figures 4.28(e)-4.28(h)**) showed a negligible difference. This suggests that similar tribo-chemical reactions occurred on steel–steel friction pairs in all tested friction processes. Thus, it can be concluded that as an additive, it is the shape and size of MWCNTs that play a great role in the friction-reduction and anti-wear properties, rather than the chemical reactions [149].

4.2.2.3. Dispersion analysis of MWCNTs in PAOs

The dispersion performance of nanolubricants is a crucial parameter related to their long-term usage in tribological applications. The sedimentation method is the easiest way to probe the dispersion stability of nanolubricant. Sedimentation is the process of nanoparticles settling down or being deposited as sediment at the bottom of the base oil. The dispersion stability is a function of the natural attributes of nanoparticles, namely, size, shape, and concentration in base oils, which affect the sedimentation velocity of nanoparticles in the oil medium. The sedimentation velocity of nanoparticles in lubricant can be estimated using Stoke's law [68] as given in Eq. (4.2):

$$V_s = \frac{gd^2}{18\eta_0}(\rho_M - \rho_L) \quad (4.2)$$

Where V_s represents the sedimentation velocity. η_0, d and g express the dynamic viscosity of lubricant (PaS), outer diameter of MWCNTs (m), and gravitational acceleration (m/s^2), respectively. The terms ρ_M and ρ_L represent the density of MWCNTs and lubricant (kg/m^3), respectively. It is noticed that the sedimentation velocity is directly proportional to the square of nanoparticles diameter and inversely proportional to the viscosity of the lubricant. Thus, the smaller size of nanoparticles along with higher viscous lubricant leads to slow sedimentation velocity. The determined sedimentation velocities for PAO 4 and PAO 6 was 6.7×10^{-3} nm/s and 4.1×10^{-3} nm/s, respectively. The calculated sedimentation velocity was high in PAO 4 compared to PAO 6, which conveys that MWCNTs will attain less time to deposit at the bottom.

The sedimentation of MWCNTs in all tested nanolubricants was examined optically via the photography method at room temperature (~ 30 ℃) over a period of time, as displayed in **Figure 4.29**. After 24 hours, the precipitation was apparent at a dose of 0.025-0.075 wt.% of MWCNTs in PAO 4 and 0.025-0.05 wt.% of MWCNTs in PAO 6. This phenomenon of precipitation was prevailed for up to four months which is evidence of poor dispersion stability. In contrast, the homogenous dispersion of MWCNTs in PAO 6 was observed at a concentration of 0.075-0.15 wt.% even after four months (**Figures 4.29(e)- 4.29(h)**). The role of the functional group to enhance the dispersion ability of MWCNTs in PAOs has been schematically explained in **Section 4.2.1.4**.

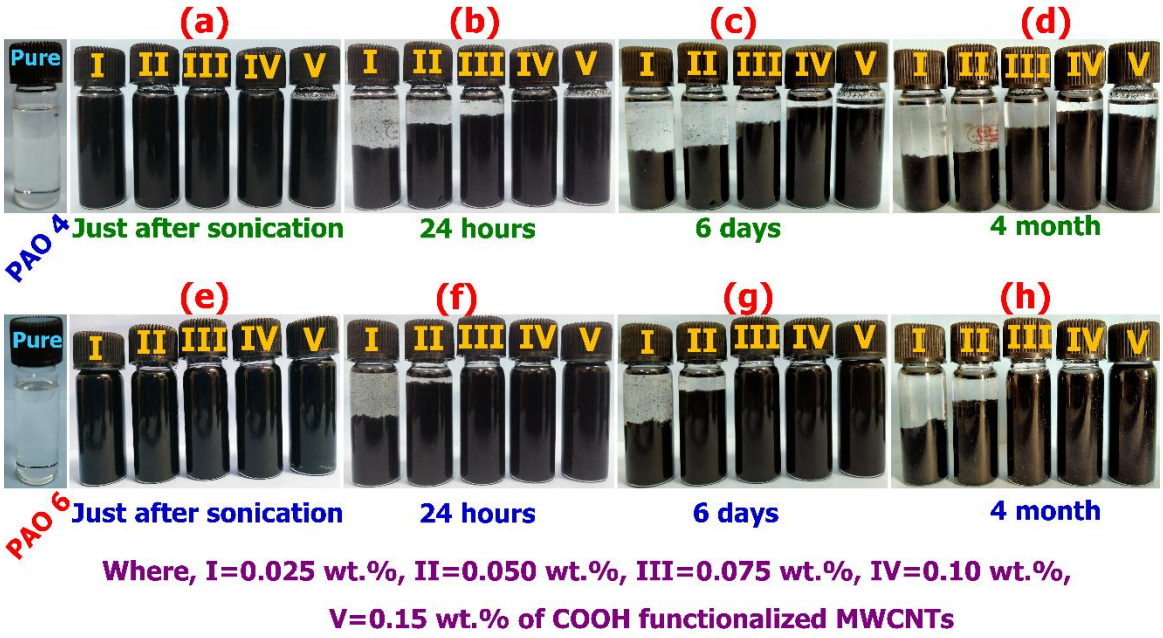

Figure 4.29: The photograph demonstrates the dispersion stability of MWCNTs (a-d) PAO 4, and (e-h) PAO 6 at room temperature (~ 30 ℃)

4.2.2.4. Rheological characterization of lubricants

The rheological behaviour of lubricants also plays a vital role in selecting the appropriate lubricant for tribological applications. All rheological characterizations were performed only on plain PAOs. It was assumed that the addition of MWCNTs in PAOs would not significantly impact the rheological characteristics because the doses of MWCNTs opted in this study were very small (i.e., 0.025-0.15 wt.%). The lubricating oil flow behaviour entirely depends on the shear rate, oil composition, and temperature. **Figure 4.30(a)** depicts the variation in shear stress as a function of shear rate at a temperature of 75℃. It is apparent from Figure **4.30(a)** that the shear stress of both PAOs increases with an increase in the shear rate. PAO 4 demonstrated higher shear stress at a low shear rate than PAO 6, but the shear stress offered by PAO 4 became more ignoble than PAO 6 at a higher shear rate and revealed a linear relationship with shear rate. The effect of the shear rate on the dynamic viscosity of PAOs is shown in **Figure 4.30(b)**. PAO 4 exhibited a higher dynamic viscosity at a lower shear rate compared to PAO 6. The dynamic viscosity of both PAOs was decreased continuously with an increase in shear rate up to 3 S^{-1} which showed a non-

Newtonian behaviour, i.e., exhibiting shear-thinning or pseudoplastic behaviour. Further increase in shear rate (from 3-100 S^{-1}), a limiting and constant value of viscosity was obtained for both PAOs, which revealed the Newtonian behaviour of PAOs. The high viscosity value at low shear rates is attributed to an elevated resistance offered by oil molecules to flow under the application of the high shear stress (**Figure 4.30(a)**) [150]. Since PAO 6 showed a lower value of dynamic viscosity at a lower shear rate than PAO 4. Thus, PAO 6 exhibited better frictional characteristics compared to PAO 4, as shown in **Figure 4.20**. Low viscosity at a low shear rate facilitates abate viscous friction and frictional power losses in automotive engines. At higher shear rates, the oil molecules get aligned, and the maximum possible shear structuring of oil molecules is attained. Further shear structuring of the oil molecules is not possible, resulting in the constant viscosity-shear rate relationship [151].

Apart from flow behaviour (shear-dependent dynamic viscosity properties), the viscoelasticity of lubricating oil is also a prominent attribute. Therefore, the storage modulus (G') and loss modulus (G'') of both PAOs were evaluated as functions of angular frequency and are arranged in **Figure 4.30(c)**. The G'' of both PAO were determined to be considerably higher than G' within the whole frequency range. This indicates that both PAOs can be regarded as viscous liquids. Although, $G'$and G'' related to PAO 6 are slightly higher within the entire frequency range than PAO 4, which signifies that PAO 6 is much thicker (more viscous) than PAO 4, also reported in **Table 3.1**. In the case of plain base oils, the loss modulus governs the tribological performance of lubricating oil. The lubricating oils with a high loss modulus exhibit excellent potential to form a tribo-film compared to lubricating oil having low loss modules. However, adding a significant additive concentration in base oil may change the viscoelastic properties of lubricating oil [152]. PAO 4 with a low loss modulus demonstrated higher wear and friction, imputing to

the poor tendency to form a lubricious thin film (Figure 4.20). Meanwhile, **Figure 4.30(d)** shows the effect of angular frequency on the dynamic viscosity of PAOs, which can be corroborated by the behaviour featured in **Figure 4.30(c)**.

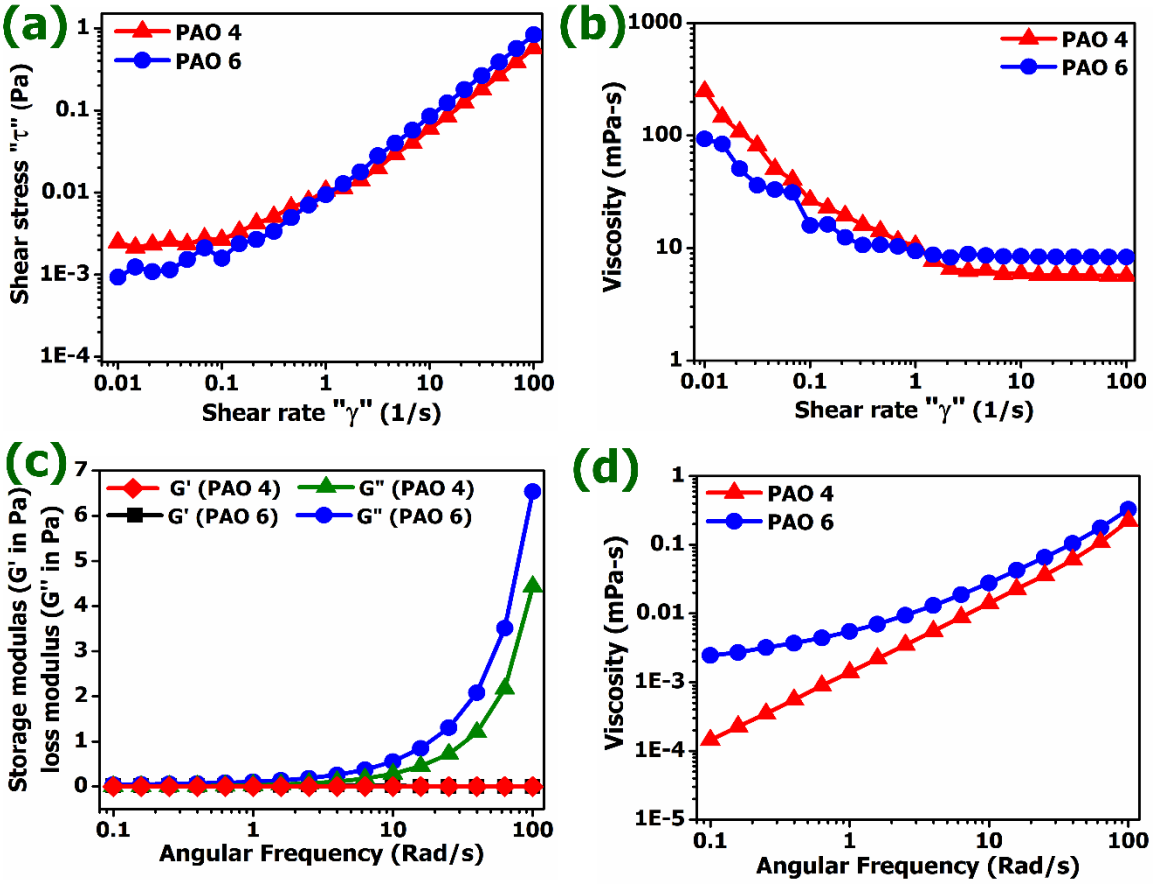

Figure 4.30: Rheological characterization of plain PAO 4, and PAO 6

4.3. Summary of the chapter

COOH-functionalized MWCNTs at different compositions (i.e., 0.025, 0.05, 0.075, 0.1, 0.15 wt.%) were dispersed in different grades of polyalphaolefins (i.e., PAO 4, PAO 6, PAO 40, and PAO 100) and polypropylene glycol (PPG 2000). In four-ball tribo-testing (i.e., fully flooded lubrication condition), the tribological performance of all PAOs was improved with the addition of MWCNTs as an additive. PAO 6 containing optimum concentration revealed the best friction-reducing ability, whereas PAO 100 exhibited the best anti-wear properties. In SRV 5 tribo-testing (i.e., starved lubrication condition), the EP

results reveal that PAO 4 and PAO 6 can sustain up to 50 N and 200 N load, respectively, without failure of lubricating film at the interface of friction pair. PAO 100 at all concentrations of MWCNTs demonstrated the best anti-friction characteristics compared to other nanolubricants, whereas PAO 4 incorporating an optimum dose of additive exhibited the best wear-reducing property among all nanolubricants. It was also observed that MWCNTs exhibited excellent anti-wear properties than friction properties.